Experimental and theoretical study of the npπ1Πu- (n 4n 4) excited states of D2: absolute absorption cross sections and branching ratios for ionization, dissociation and fluorescence

Michèle Glass-Maujean, A-M Vasserot, Ch Jungen, H Schmoranzer, A Knie, S Kübler, A Ehresmann

Experimental and theoretical study of the $np\pi\,^1\Pi_u^-$ ($n \geq 4$) excited states of D_2: absolute absorption cross sections and branching ratios for ionization, dissociation and fluorescence

M. Glass-Maujean[1*], A-M. Vasserot[1], Ch. Jungen[2,3], H. Schmoranzer[4], A. Knie[5], S. Kübler[5] and A. Ehresmann[5]

[1] Sorbonne Universités, UPMC Univ. Paris 06, CNRS, UMR 8112, Laboratoire d'Etudes du Rayonnement et de la Matière en Astrophysique et Atmosphères, F-75005, Paris, France

[2] Laboratoire Aimé Cotton du CNRS, Bâtiment 505 Université de Paris-Sud, F-91405 Orsay, France

[3] Department of Physics and Astronomy, University College London London WC1E 6BT, United Kingdom

[4] Fachbereich Physik, Technische Universität Kaiserslautern, D-67653 Kaiserslautern, Germany

[5] Institute of Physics and Center for Interdisciplinary Nanostructure Science and Technology (CINSaT), Heinrich-Plett-Str. 40, Universität Kassel, D-34132 Kassel, Germany

[*] phone number: +33(0)-1-4427-4326. e-mail: michele.glass@upmc.fr

March 18, 2015

Abstract

The absolute absorption cross section and the branching ratios for the competing decay channels fluorescence, dissociation, and ionization of photoexcited long-lived $^1\Pi_u^-$ superexcited molecular levels in

D_2 have been measured with a spectral resolution of 0.001 nm from the ionization threshold of D_2 up to the $D(n = 1)$+$D(n = 3)$ dissociation limit. The experimental energies and absorption line intensities are compared with fully *ab initio* multichannel quantum defect theory (MQDT) calculations [1] which are based on quantum-chemical potential energy curves and transition moments of Wolniewicz and collaborators [2, 3]. The overall agreement between experiment and theory is good. The branching ratios for the competing decay channels are also reproduced by the calculations including their substantial variations from level to level. A comparison of the vibronic interactions in the isotopomers H_2 and D_2 is made.

1 Graphical abstract

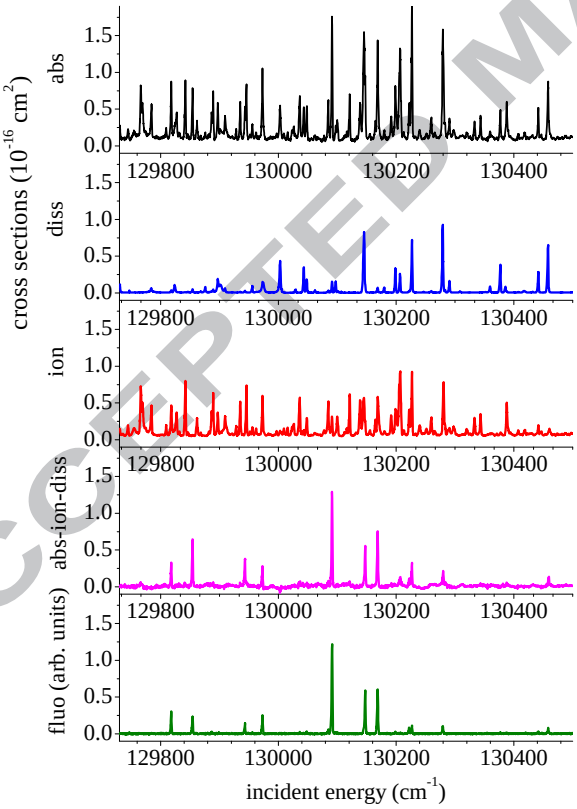

2 Highlights

- 319 photoabsorption transitions to $np\pi$ $^1\Pi_u^-$ upper levels of D_2 measured and assigned
- 141 previously unknown spectral lines observed and assigned
- Absolute absorption spectral line intensities measured
- Dissociation, ionization and fluorescence branching ratios measured
- Calculation from first principles of perturbed intensities and transitions

3 Introduction

This paper is the second in a series [4] describing a joint experimental and theoretical effort which aims at a detailed understanding of the high-resolution absorption spectrum of molecular deuterium at room temperature. The present work is focused on the study of absorption line intensities and decay dynamics involving $^1\Pi_u^-$ excited states. The $^1\Pi_u^-$ excited levels of D_2, just as those of H_2, are the main contributors to the fluorescence processes which take place above the ionization threshold. These photon emission processes are important in the context of astrophysics and for plasma diagnostics [5]. The $^1\Pi_u^-$ excited states of molecular hydrogen and deuterium are also interesting from a theoretical point of view. They are Rydberg states in which the $p\pi$-type Rydberg orbital ($\ell = 1$) is oriented perpendicular to the molecular axis and to the rotational plane and therefore is only little affected by molecular vibration and not at all by molecular rotation. These excited states are subject to weak vibronic interactions which are responsible for most of the interesting and complex excited-state dynamics. The present work leads to insight into this dynamics in D_2 and allows an interesting comparison with the isotopomer H_2 to be made (Sec. 8).

We present here experimental data obtained with a setup designed for combined absorption, ionization yield, and fluorescence measurements. This experimental technique is complementary to the Fourier-Transform (FT) experiment carried out with the SOLEIL synchrotron which has been described in the preceding paper [4]. While the FT experiments yield highly accurate energy level positions, they do not provide absolute transition intensities and are unable to give much insight into the decay mechanisms. By contrast, the monochromator experiments reported here, albeit less accurate in terms of spectral energy resolution, enable the absolute absorption cross sections for the individual spectral lines to be determined. In addition they provide the

cross section values for the three possible decay channels: fluorescence, dissociation and ionization.

We also present multichannel quantum defect theory (MQDT) calculations of the excited state level energies and their transition probabilities to the ground state [1]. These results yield good overall agreement with the measured values - in fact they greatly aid the spectral analysis - and in addition they reproduce the balance between the competing decay processes including its significant evolution from level to level.

4 Experimental aspects

The experimental setup has been described in detail in previous publications (see e.g. [6, 7, 8]). Briefly, the VUV photons coming from the undulator beamline U125/2-10m-NIM of BESSY II are dispersed by a 10 m-normal-incidence monochromator equipped with a 4800-lines/mm grating giving a spectral resolution of 2 cm^{-1} (0.001 nm) in first order; this value represents the convolution of the apparatus function with the Doppler width at room temperature. The uncertainty of the scan linearity (1 cm^{-1}) is the main source of error in the energy measurement. A photodiode located at the back of the gas-target cell enables the detection of the transmitted light. The intensity of the incident light can be monitored by the ionization signal from the last refocussing mirror of the beamline in front of the cell. A small voltage of 10 V was applied to an electrode in the target cell in order to attract the photoions. The Ly_α fluorescence emitted from the H($n = 2$) fragments was detected by a microchannel-plate detector (Hamamatsu F1552-01 Inconel) at the magic angle with respect to the E-vector of the synchrotron radiation in order not to detect any polarization effects. A MgF_2 window in front of the detector was used to ensure that no charged fragment or Ly_β fluorescence from H($n = 3$) fragments could reach the detector. All signals mentioned above, i.e. the photoion yield, the fluorescence yield, the photoelectric current from the refocussing mirror (incident light intensity) as well as the transmitted light intensity coming through the target cell, were recorded simultaneously as functions of the incident photon energy. As a result, the ionisation and dissociation excitation spectra and the absorption spectrum could be recorded simultaneously.

The intensities of the absorption spectrum, recorded at high spectral resolution, have been calibrated directly, based on the known absorption path length and the known gas pressures of 20 or 10 mTorr (2.67 or 1.33 Pa), respectively, at room temperature (300 K). The photoionization and photodissociation excitation spectra have been calibrated directly by use of transitions

known to produce only photoionization or photodissociation. The Ly_α detection efficiency was determined by comparing the absorption and dissociation structures in the spectrum at specific wavelengths for which it is known that the lines under consideration are totally predissociated. This is the case for the $D\ ^1\Pi_u^+ \rightarrow X\ R(1)$ transitions [6]. In order to cross-check the various calibrations, we have recalculated the absorption cross section as the sum of the dissociation and ionisation cross sections. The only lines for which the absorption cross section could not be reproduced correctly in this way are transitions - mostly Q lines - which lead to molecular fluorescence. For these, the experimental fluorescence cross section has been determined subsequently from the difference spectrum obtained by subtracting the sum of the dissociation and ionization cross sections from the absorption cross section. *A priori* the directly recorded visible fluorescence excitation spectrum does not provide this information because this visible fluorescence populates levels of the E, F excited state in addition to the G, K excited state (see Ref. [6] for a more complete discussion). Fig. 1 displays a section of the experimental spectra obtained with the BESSY setup.

5 Theoretical approach

As in the preceding paper [4] we have used multichannel quantum defect theory (MQDT) to evaluate transition energies and probabilities from first principles. The implementation of the MQDT formalism used here has been described in Refs. [9] and [6]. For details we refer the reader to the discussion and further references given there. Briefly, the main ingredients are energy- and nuclear-coordinate-dependent quantum defects $\mu(\epsilon, R)$ and dipole absorption transition moments $d(\epsilon, R)$ [6] which embody the dynamics of all processes considered here. These parameters are extracted from *ab initio* potential energy curves $U_{np\pi}(R)$ and state-to-state absorption dipoles $D_{np\pi \leftarrow X}(R)$ [2, 3]. The quantum defect and transition moment functions are converted into energy-dependent vibronic channel interaction quantum defect matrices $\mu_{v^+N^+,v^{+\prime}N^{+\prime}}$ and channel transition moments $d_{v^+N^+ \leftarrow X,v''=0,N''}$ which are then injected into the rovibronic MQDT calculations.

In the discrete range - or when open ionization channels are omitted from the treatment (e.g. for the purpose of identifying the resonances present in a given range) - the MQDT procedures yield the spectrum of rovibronic energy levels $E_{n,v,N}$ as well as the rovibronic transition moments $D_{n,v,N}$ for the absorption transitions leading to them. Note that due to vibronic mixing the vibronic label nv has no strict meaning in general but is useful for bookkeeping purposes. On the other hand of course the upper state total

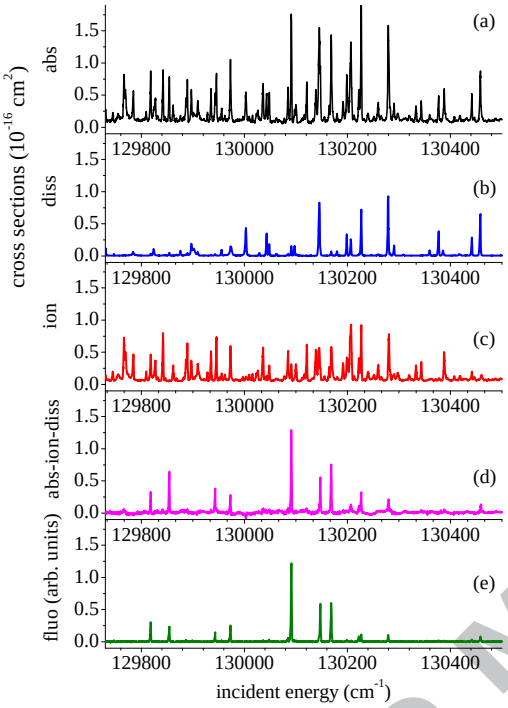

Figure 1.
(Color online) A section of the D_2 absorption and photoexcitation spectra recorded at BESSY. (a) (black online) absorption, σ_{abs}. (b) (blue online) dissociation, σ_{diss}. (c) (red online) ionization, σ_{ion}. (d) (violet online) $\sigma_{fluo} = \sigma_{abs} - \sigma_{diss} - \sigma_{ion}$. (e) (green online) fluorescence.

angular momentum N (exclusive of spins) as well as the total parity remain well-defined. The transition moments $D_{n,v,N}$ are converted into upper-state spontaneous emission probabilities A by means of the relation

$$\begin{aligned} A_{n,v,N\rightarrow X,v''=0,N''} &= 4\,\frac{mc^2}{\hbar}\,\alpha^5\left(\frac{E_{n,v,N}-E_{X,v''=0,N''}}{2\mathcal{R}hc}\right)^3\left(\frac{1}{2N+1}\right)\left|\frac{D_{n,v,N}}{a_0}\right|^2. \\ &= 6.426\cdot 10^{10}\left(\frac{E_{n,v,N}-E_{X,v''=0,N''}}{2\mathcal{R}hc}\right)^3\left(\frac{1}{2N+1}\right)\left|\frac{D_{n,v,N}}{a_0}\right|^2 \text{ s}^{-1}, \end{aligned} \tag{1}$$

where α is the fine structure constant and $\mathcal{R}$ is the Rydberg constant, while m, c, h and a_0 have their usual meanings. For the $Q(N'')$ transitions studied here one has $N = N''$.

The radiative lifetime τ_{fluo} of a given excited level n, v, N to the X ground

state is evaluated according to

$$\frac{1}{\tau_{fluo}} \simeq A_{n,v,N\to X} \simeq \sum_{v'',N''} A_{n,v,N\to X,v'',N''} \ , \qquad (2)$$

where $A_{n,v,N}$ are the Einstein coefficients for spontaneous emission from Eq. (1). The sum over the ground state vibration-rotation levels in Eq. (2) is carried out within the MQDT approach by use of Eq. (1) for $v'' > 0$, with the help of computed vibrational wavefunctions for the X ground state, thereby also taking account of the $R-$ dependence of the transition moment function. The expression Eq. (2) does not account for emission to the E, F or G, K levels, nor does the sum over v'', N'' explicitly include emission to the vibrational continuum of the X state. The former occurs in visible or infrared spectral regions and therefore is weakened by the cubic energy factor. The latter amounts to less than a few % for excited state levels with $v > 14$ as may be concluded from inspection of the Franck-Condon factors. As a consequence, Eq. (2) constitutes a good approximation for the theoretical determination of the fluorescence widths $\Gamma_{fluo} = 1/2\pi c\tau_{fluo}$, in cm^{-1}, of the excited state levels.

When open ionization continua are present and included in the treatment, the continuum eigenphases and ionization cross section profiles are evaluated as described in Ref. [6]. The autoionization partial widths Γ_i can then be evaluated directly by inspection of the ionization cross section profiles or alternatively from the energy-derivative of the eigenphase-shift sum.

We have not evaluated the photodissociation partial cross sections in the present work as this channel plays only a marginal role in the experimental data at hand. The only exceptions where dissociation is observed are a few of the very highest energy levels identified here, which may dissociate into D($n = 3$)+D($n = 1$)). We nevertheless like to mention that partial dissociation widths for the narrow resonances discussed in this work may be obtained efficiently within the same MQDT approach, with no additional physical quantities involved. The method is based on a stabilization procedure and has been outlined in Ref. [6].

With regard to the more technical aspects of the calculations we may say that the energy level calculations converged satisfactorily and proved stable when the conditions of the computations were varied (e.g. the number of Rydberg channels v^+ included, the cutoff point chosen for the vibrational wavefunctions at large internuclear distance). By contrast, the calculated intensities were found to depend more sensitively on the precise conditions in which each computation was carried out. We estimate that the calculated intensities are probably accurate to only about 10 to 20%. The resulting

theoretical transition energies and intensities as well as the partial ionization widths have already been described [1, 4].

Once the partial widths Γ_{ion}, Γ_{fluo} and Γ_{diss} have been calculated for a given excited level as just outlined, the theoretical branching ratios for its decay are obtained according to

$$\gamma_{ion} = \frac{\Gamma_{ion}}{\Gamma_{fluo} + \Gamma_{diss} + \Gamma_{ion}} \tag{3}$$

(and analogous expressions for γ_{fluo} and γ_{diss}), where Γ_{fluo}, Γ_{diss} and Γ_{ion} are the partial fluorescence, dissociation and ionization widths, respectively, with the total level width Γ being given by $\Gamma_{fluo} + \Gamma_{diss} + \Gamma_{ion}$. Eq. (3) is appropriate for the description of slowly decaying levels as we have here, although it may fail for broad decay profiles or complex resonance features.

6 Experimental determination of radiative lifetimes and branching ratios

The measured absorption cross section σ has been integrated over the profile of each spectral line, to yield an experimental value for the integral on the left hand side of the following expression:

$$\int \sigma d\omega = \frac{1}{8\pi c\omega^2} A_{n,v,N\rightarrow X,v''=0,N''} \frac{2N+1}{2N''+1} n_{N''} \ . \tag{4}$$

Here $\omega = (E_{n,v,N} - E_{X,v''=0,N''})/(2\mathcal{R}hc)$ is the incident photon energy in cm^{-1}, and $n_{N''}$ is the fraction of molecules in the rotational state N'' in the vibrational ground state at the given temperature of 300 K. An experimental value for the Einstein coefficient for each transition is obtained from Eq. (4) by solving for A.

In practice the spectral resolution of the present experiment is not sufficient to allow the determination of the level width Γ directly from the observed absorption profile. Therefore Eq. (3) cannot be used for the determination of the branching ratios. Instead, experimental values for these quantities are obtained as follows. Once the total absorption cross section has been determined from the integrated cross section profile of a given spectral line in the absorption spectrum to yield the Einstein coefficient A as just described, the partial cross sections are evaluated from the ionization, dissociation or difference spectrum, respectively. Then the following expression (5) is utilized, which relates the measured partial cross section and A value

to the branching ratio γ for a given decay channel, e.g.:

$$\int \sigma_{ion}\, d\omega = \frac{1}{8\pi c\omega^2}\, \gamma_{ion}\, A_{n,v,N\to X,v''=0,N''} \frac{2N+1}{2N''+1} n_{N''}\ , \qquad (5)$$

This expression differs from Eq. (4) by the additional branching ratio factor γ_{ion}, and analogous expressions hold of course for the fluorescence and dissociation branching ratios, γ_{fluo} and γ_{diss}, respectively. σ_{ion} is the measured ionization cross section to be integrated over the profile of a given peak, whereas the A coefficient has been determined from Eq. (4) as just stated.

7 Results

The results obtained for the $3p\pi D$ state have been published previously [10]. For the $np\pi\,^1\Pi_u^-$ levels with $n \geq 4$, the positions, widths and integrated peak intensities (peak areas) have been determined from Gaussian fits of the peaks observed in the absorption spectrum, the dissociation and ionization excitation spectra, as well as from the difference spectrum (as defined in Sec. 2). This analysis yields the level energies, the Einstein coefficients A and the branching ratios for the different decay channels, which may then be compared to the theoretical values calculated by MQDT.

The main problem encountered in this procedure arises from line blending. Some groups of spectral lines which are resolved in the FT spectrum appear blended in the BESSY spectrum so that the fitting procedure becomes ill defined as it involves too many fit parameters. However, this difficulty may be overcome in many cases by making extensive use of the information included in the various decay channels monitored in the BESSY experiment. For instance, a given transition may appear blended in absorption whereas it is resolved in one of the decay channels. It is then possible to reduce the number of fit parameters and to extract meaningful values for the various quantities. The uncertainty of the intensities was taken as three times the statistical error, with an added uncertainty corresponding to the estimated calibration error of 10%.

The observed transition energies with the assignments, the corresponding residuals observed - calculated, the calculated and measured Einstein coefficients A for the Q transitions to the ground state vibrational level $v'' = 0$ are listed in Tabs. 1 to 5. The tables also contain the branching ratios for the decay of the excited levels which have been extracted from experiment. The corresponding theoretical values are not given in the tables, but are represented graphically in Fig. 6.

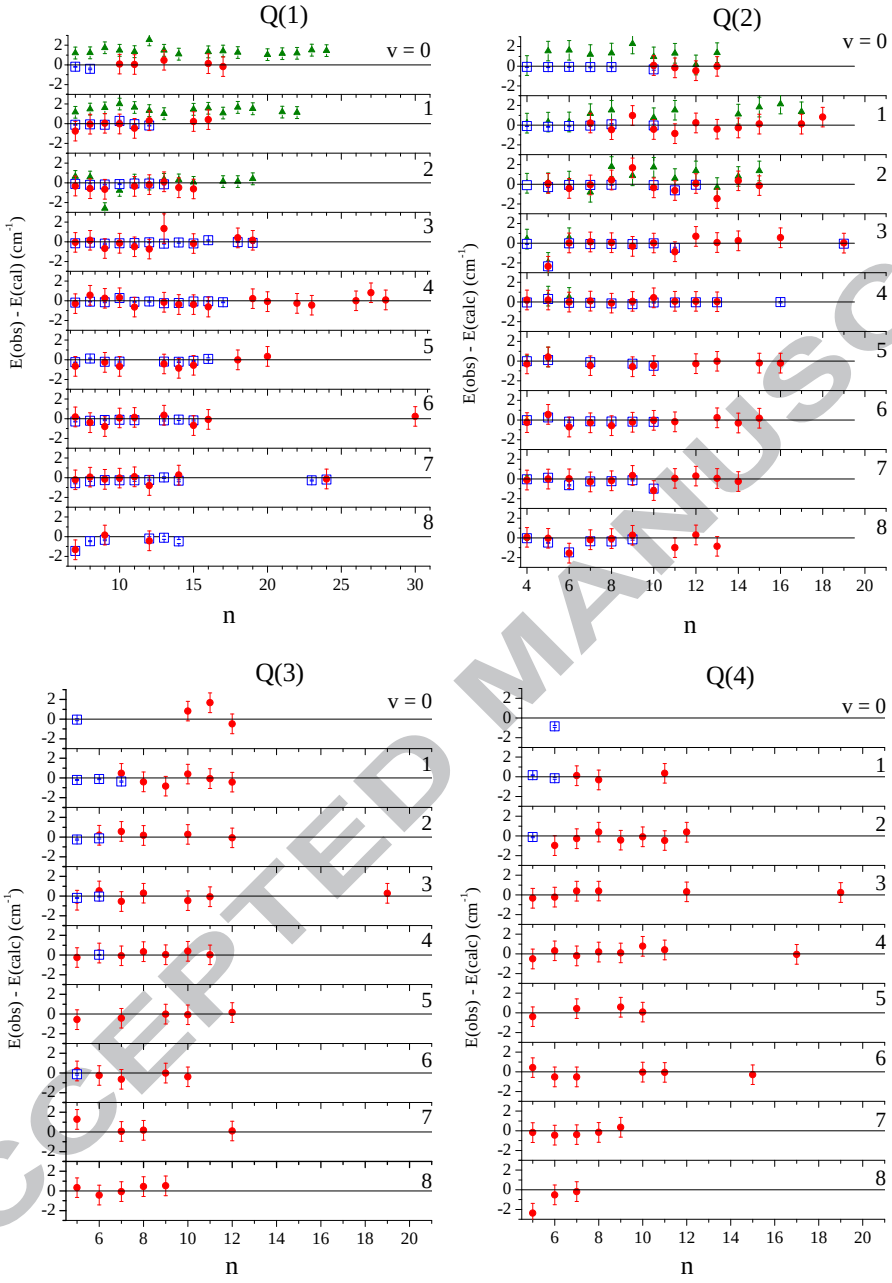

Figure 2.
(Color online) Deviations observed-calculated for the $Q(N'')$ $(N'' = 1 - 4)$ transitions to the vibrational levels v of the $np\pi$ states of D_2 plotted as function of the principal quantum number n. Full circles (red): present measurements - present MQDT calculations. Triangles (green): experimental values from [11] - MQDT. Open squares (blue): experimental values from [4] - MQDT.

7.1 Level energies

We have found that whenever a transition has been observed both in the SOLEIL and BESSY experiments, the peak positions agree, with the SOLEIL FT values being of course far more accurate. However, as the BESSY measurements are more sensitive and the temperature used was higher, the new BESSY measurements extend the SOLEIL measurements toward the levels with higher values of the principal quantum number n, vibrational quantum v and rotational quantum number N. Figure 2 displays the deviations of the resulting transition energies from those obtained by means of the MQDT calculations for $N = 1$ to 4 for various values of n and v. The figures also include the deviations obtained when previously measured values are used [11]. The figures demonstrate that the present measurements of transition energies are consistent with the previous data where these are available. In all, the BESSY spectrum has enabled 143 new excited state levels to be determined: 12 levels for $N = 1$, 28 for $N = 2$, 45 for $N = 3$, 42 for $N = 4$ and 16 for $N = 5$, respectively. Figure 2 also demonstrates that the agreement between calculations and measurements is satisfactory in all cases. In the following we present some details concerning the levels associated with the various upper state Rydberg members n.

7.1.1 The $4p\pi D'$ state

The rovibronic level structure of the $4p\pi D'$ state has been studied previously in Refs. [1, 4, 11, 12, 13]. For $N = 1$ and 2, the present measurements agree with the FT previous values to within the present larger uncertainty. Three new upper state levels have been identified, namely $v = 16$, $N = 2$ and $v = 17$, $N = 1$ and 2. Further, five $N = 3$ levels which had not been observed in the FT spectrum could now be measured at BESSY. Four of them have been seen previously in emission [13], and three of these, for $v = 8$, 10 and 12, agree with the previous measurements. For $v = 11, N = 3$, however, we observe two spectral lines located at 131992.4 cm^{-1} and at 131995.9 cm^{-1}, respectively, symmetrically displaced to each side of the theoretical position 131994.0 cm^{-1}. These two lines have comparable intensities. It is likely that they result from a local perturbation by a level not predicted by our MQDT calculation. The perturbing level may well belong to the nf manifold of Rydberg states (possibly with $n \approx 4 - 5$) which is not included in our theoretical treatment. The previously published value [13] for $v = 11, N = 3$ corresponds to 131993.34 (± 0.3 cm^{-1}) and agrees with the lower of the two transitions which we observe. Local perturbations of this type occur recurrently in the spectrum of diatomic hydrogen, e.g. in the $5p\pi$ state of H_2

where several such situations have been identified [14]. The $v = 13, N = 3$ value is new. Our results for $N = 4$ are fully consistent with those of Ref. [13] for $v = 6$ to 10 and 12, while our assignments for $v = 11$ and 13 are new. Similarly for $N = 5$ our results are consistent with those of Ref. [13] for $v = 4$ to 7, 9 and 10, while our assignment for $v = 8$ is new.

In summary, our calculations reproduce the $4p\pi D'$ levels very well up to $v = 11$, close to the dissociation threshold D($n = 3$) +D($n = 1$) ($\simeq$ 134200 cm^{-1}). For $v \geq 12$ the classically accessible range of internuclear distances starts to extend into a region where the D' state no longer corresponds to a pure p configuration in contrast to the assumption underlying our theoretical treatment. This point has already been discussed in the preceding paper [4].

7.1.2 The $5p\pi D''$ state

For $N = 1$ and 2 and all v values the BESSY measurements are consistent, to within their larger uncertainty, with the FT values determined in Ref. [4]. For $N = 3$ we add here five new assignments ($v = 7 - 11$). Similarly for $N = 4$ and 5 we extend here the range of known values by adding six ($v = 6-9$ and 11) and four new assignments ($v = 3, 4, 7$ and 8), respectively. Once again, the calculations reproduce the experimental energies very well except for the $v = 3, N = 2$ and $v \geq 8, N = 4$ as has already been discussed in the preceding paper.

7.1.3 The $np\pi$ states with $n \geq 6$

No less than 120 new assignments of $np\pi$ levels with $n \geq 6$ have emerged from the present analysis, as a consequence, no doubt, of the high sensitivity of the BESSY experiment. The residuals $|E(\text{obs}) - E(\text{calc})|$ remain below 1 cm^{-1} for all of these, that is, these levels are reproduced by the calculations to within the experimental uncertainty.

7.2 Line intensities

The experimental Einstein coefficients A determined according to Eq. (4) are here compared with the theoretical values which were previously evaluated [1] with the same MQDT approach used here.

7.2.1 Transition intensities involving the $4p\pi D'$ state

Fig. 3 displays the comparison between experiment and theory for 49 $Q(N)$ transitions leading to the upper $4p\pi D'$ state. By and large, experiment and theory are seen to be in good agreement both with regard to the overall

trend - which represents a Franck-Condon envelope - and to local vibronic perturbations. Examples of the latter occur for $v = 8$ and 9 where the upper levels are affected by interactions with the nearby $3p\pi D, v = 13$ and $v = 14$ levels, respectively. A small discrepancy, hardly visible on the graph of Fig. 3, occurs for the $Q(3)$ $v = 11$ transition which is split into two components as noted above. For the purposes of comparison the calculated A values of the $Q(1)$ $4p\pi, v = 10$ and $12p\pi, v = 5$ transitions have been summed up because the observed lines appear completely blended in the BESSY spectrum and their upper levels are in fact mixed. The calculations predict the two lines to appear with a separation of 0.5 cm^{-1}.

It is instructive to compare the variations of the A coefficients with the vibrational quantum number v for D_2 displayed in Fig. 3 with those observed in the isotopomer H_2 [15]. It turns out, not really unexpectedly, that while the overall behavior is similar, the perturbations do not occur for the same v values. What is more intriguing is that the perturbations are stronger in D_2 despite the fact that the non-adiabatic vibronic coupling is intrinsically weaker in D_2 due to the larger nuclear mass. The reason must be that the local perturbations are stronger in the heavier isotopomer because the perturbing levels lie closer to each other.

7.2.2 Transition intensities involving the $5p\pi D''$ state

Fig. 3 compares the theoretical and the experimental values of the Einstein A coefficients for 40 $Q(N)$ lines leading to levels associated with the $5p\pi$ D'' upper state. The experimental and the calculated values are once again seen to be in satisfactory agreement. In some instances the experimental value lies higher than the theoretical prediction. This is probably caused by spectral blending in the experimental spectrum with transitions not considered here. The opposite occurs for the $Q(2)$ $v = 3$ transition where the experimental value is much smaller than predicted. It turns out that this is another example of a local interaction with an unknown perturber. Indeed, we observe no line at the calculated frequency, but instead a symmetrically displaced doublet of lines whose intensities are comparable. Summing the two intensities up would bring experiment and theory essentially into agreement, but we have not done this in Fig. 3 since the perturber level has not been identified at this point. We follow Ref. [11] here by assigning the lower frequency transition to the $Q(2)$ the $5p\pi D'', v = 3$ transition. The overall dependence of the Einstein A values as function of v represents again approximately a Franck-Condon envelope. It exhibits strong perturbations around $v = 6$ for all N values, due to interaction with $8p\pi, v = 4$ and $6p\pi, v = 5$. A further complication arises because all these upper levels in turn are immersed in a

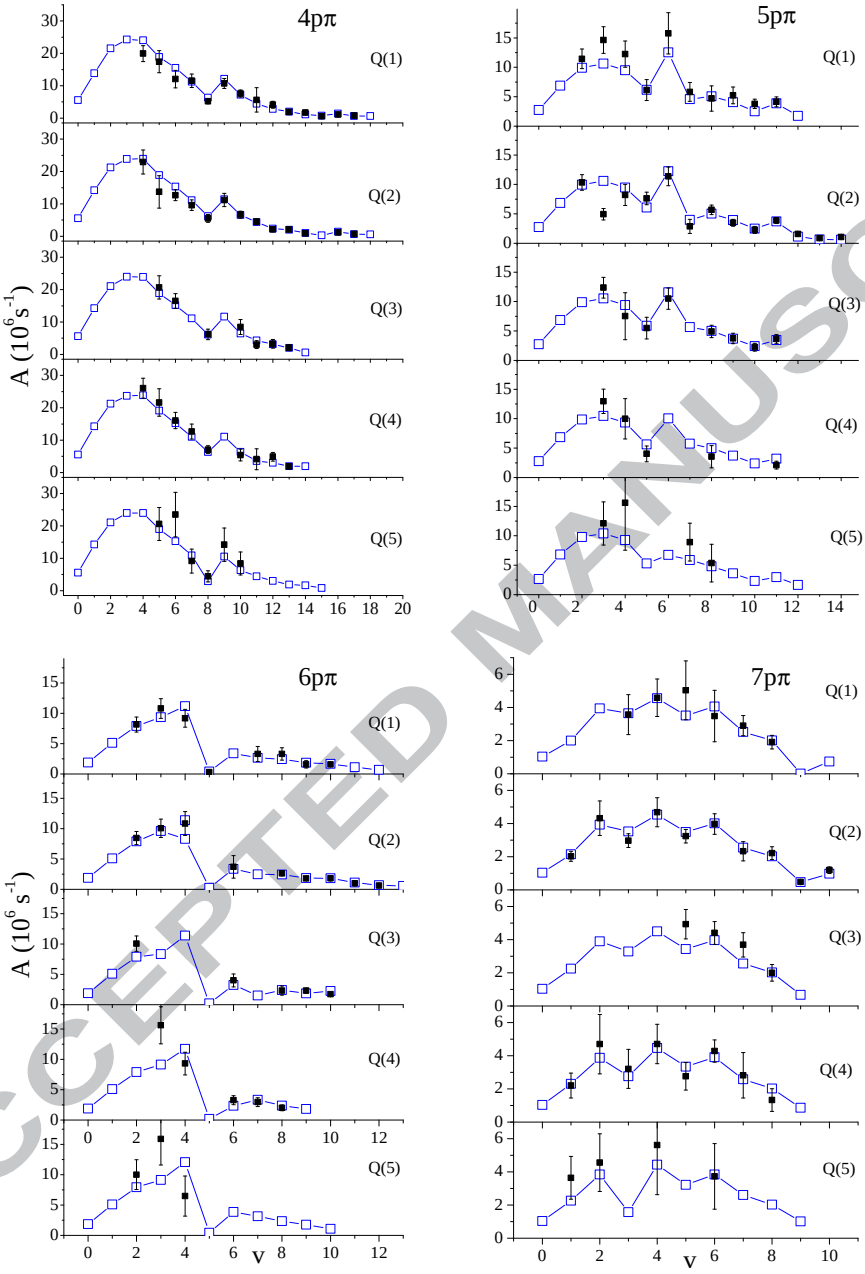

Figure 3.
(Color online) Einstein coefficients A for the $Q(N)$ transitions from $v'' = 0, N''$ levels of the X ground state to the $np\pi, v, N = N''$ $(n = 4 - 7)$ upper levels, plotted versus the upper vibrational quantum number v. Filled squares (black): present experimental values. Open squares (blue) connected by full lines: calculated values.

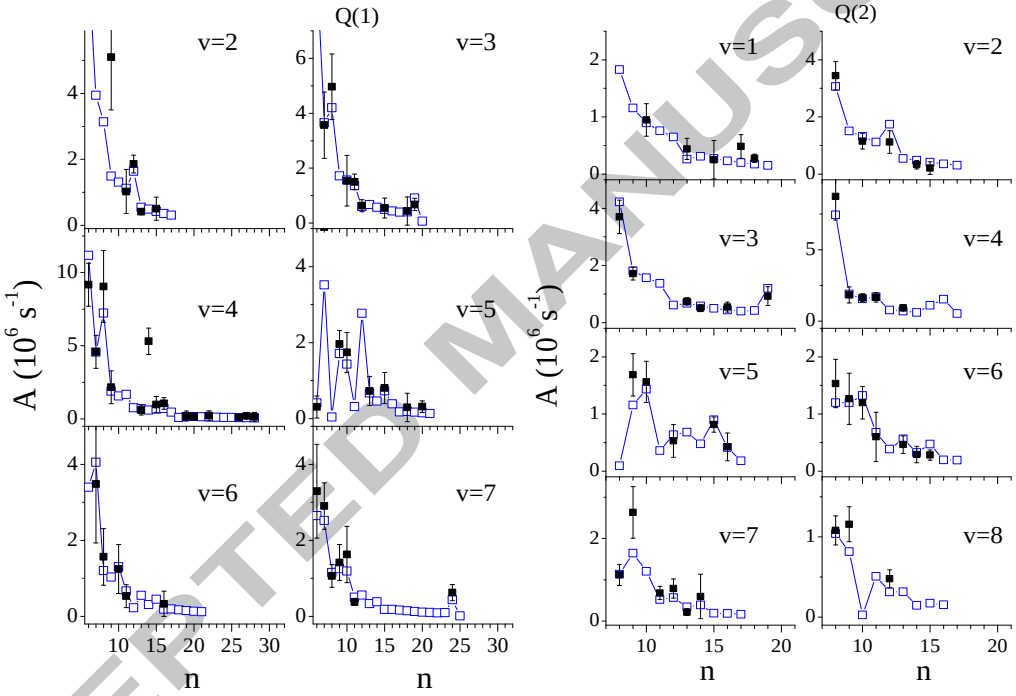

Figure 4.
Einstein coefficients A for the $Q(1)$ and $Q(2)$ transitions $np\pi, v - X, v'' = 0)$ plotted versus n. Symbols as in Fig. 3.

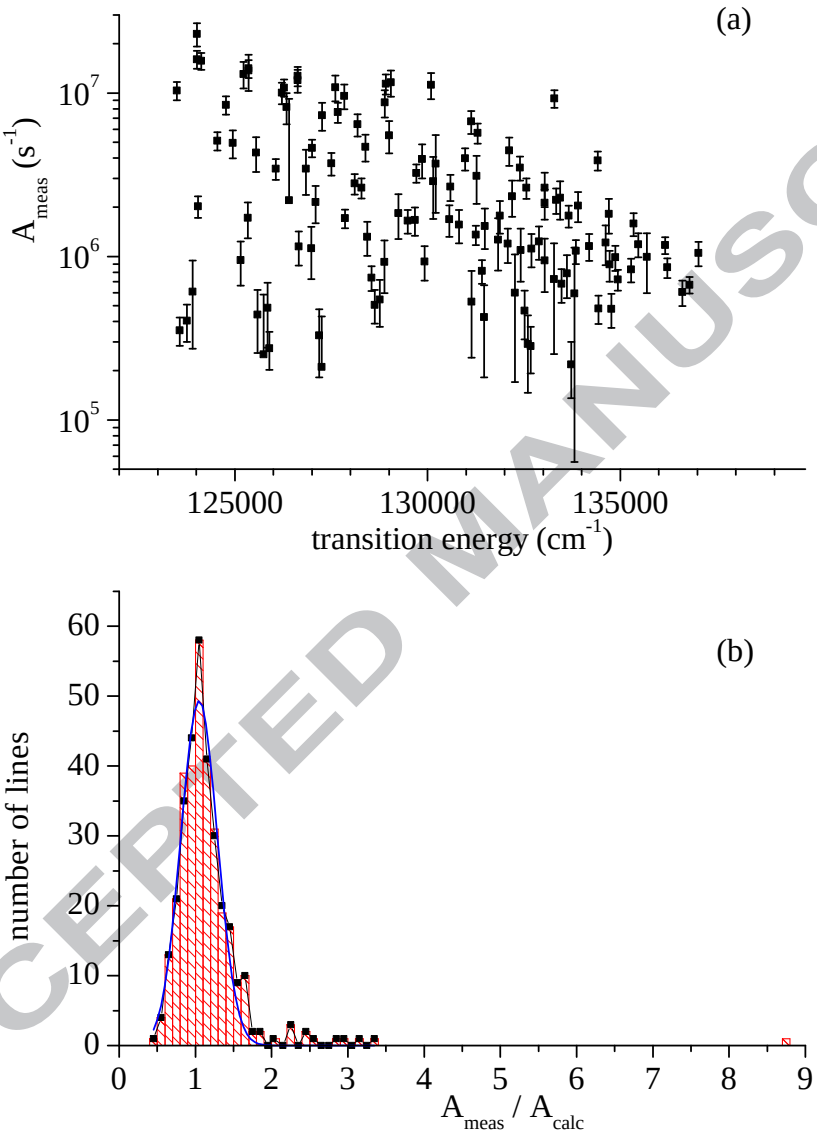

Figure 5.
(a) Einstein coefficients A measured for $Q(2)$ transitions in D_2. (b) Histogram of the ratios of the measured values over the calculated ones, A_{meas}/A_{calc} for 319 $Q(N'')$ transitions. The full curve represents a fit to a Gaussian function.

quasi-continuum of high-n $np\pi, v = 3$ Rydberg levels. This complex perturbation pattern is well reproduced by the calculations. Once again the comparison with H_2 is instructive [14] and shows that the perturbations are not located at the same v values ($v = 2$ for H_2 versus $v = 5$ and 6 for D_2) and are stronger in D_2 as compared to H_2.

7.2.3 Transition intensities involving the $6p\pi$ state

The comparison between calculated and measured values of the Einstein coefficients A is displayed in Fig. 3 for 30 $Q(N)$ transitions. The experimental values are seen to agree rather well with the theoretical predictions. Striking perturbations occur for $v = 5$ and are due to $5p\pi, v = 6$. The interference reduces the intensities by several orders of magnitude in all cases so that the lines could not be detected at all in the spectrum. The perturbation effects are more obvious than in H_2 where the line intensities exhibit a smoother overall behavior [16].

The $6p\pi, v = 3, N = 2$ upper level is embedded in the dense manifold of the $np\pi, v = 2, N = 2$ upper state Rydberg levels with high n, and is calculated to coincide nearly with $29p\pi, v = 2, N = 2$. The energy separation is calculated to amount to only 0.5 cm^{-1}, and the lines are indeed not resolved by our experiment. In Fig. 3 the experimental intensity is compared with the sum of the calculated values of the two lines. A more extreme example of a perturbation of an excited level with a dense manifold of perturbers is seen in the $Q(1)$ $v = 3$ transition where the observed peak according to the calculations corresponds to a 'complex' resonance with component levels having principal quantum numbers as high as $n \approx 150$. This has already been discussed in the preceding paper. Fig. 3 compares the experimentally determined intensity with the calculated values summed over all the interacting components because these latter cannot be distinguished in the experiment.

7.2.4 Transition intensities involving the $7p\pi$ state

Fig. 3 illustrates the comparison of experiment and theory for the intensities of 32 $Q(N)$ transitions. The agreement is good and no further comment is required.

7.2.5 Transition intensities involving $np\pi$ levels with $n \geq 8$

Unlike in the preceding figures where the intensity distribution was plotted as a function of the upper state vibrational quantum number v, Fig. 4 consists of sets of plots, for $Q(1)$ and $Q(2)$ transitions and for various values v, where the intensity distribution is plotted as function of the upper state

principal quantum number n. Therefore instead of a Franck-Condon pattern one may expect the distributions to follow the Rydberg n^{-3} scaling law. The figures demonstrate that although the overall trend does follow the scaling law, the widespread perturbations cause strong irregular deviations from it. The MQDT calculations reproduce these perturbations, and the agreement between experiment and theory is good. The $Q(3)$ and $Q(4)$ transitions (not shown in the figures) exhibit a similar apparently erratic behavior, but which is again reproduced by the calculations.

Exceptions are two $Q(1)$ transitions and one $Q(3)$ transition which exhibit intensities far stronger than calculated by MQDT, without any coincidence being predicted. These are the $Q(1)$ $9p\pi, v = 2$ and $Q(1)$ $14p\pi, v = 4$ transitions and the $Q(3)$ $11p\pi, v = 0$ transition. These spectral lines may well be blended with extra lines which do not belong to the np manifold, similarly as in H_2 where a number of such cases has been documented [6, 17].

7.2.6 Summary of intensity analysis

In all, we have measured the intensities of 319 Q transitions whose A coefficients vary from $2 \cdot 10^5$ to $2 \cdot 10^7$ s^{-1}, i.e. over two orders of magnitude. This fact is illustrated by the semi-logarithmic plot of Fig. 5(a), and underlines the range of sensitivity of the present measurements. Fig. 5(b) is a histogram of the ratios of the measured and calculated A coefficients, for all 319 spectral lines discussed here. The distribution can be fitted by a Gaussian function (black continuous line in the figure), which is centered at 1.05 ± 0.25 and has a width of 0.48. Note that the histogram has been drawn without taking account of the experimental uncertainties, a procedure which probably is the main cause for the relatively large width of the Gaussian distribution. Numerical shortcomings of the calculations may also be in part responsible for the width of the distribution (cf. Sec. 5).

A number of outliers are also visible in the plot. Most of them, which are located between 2 and 3 on the abscissa, are clearly due to spectral blending. The outermost points in the plot, near 3.4 and 8.7, respectively, correspond to the above mentioned $Q(1)$ $9p\pi, v = 2$ and $14p\pi, v = 4$ lines which have already been discussed.

7.3 Line widths

No broadening has been observed on any $Q(N)$ line in the BESSY spectra. The calculated values of the ionization widths of the $np\pi$ ($n \geq 4$) levels are less than 0.5 cm^{-1} [4], that is, their natural width is indeed calculated too small to be detected by the present experiment.

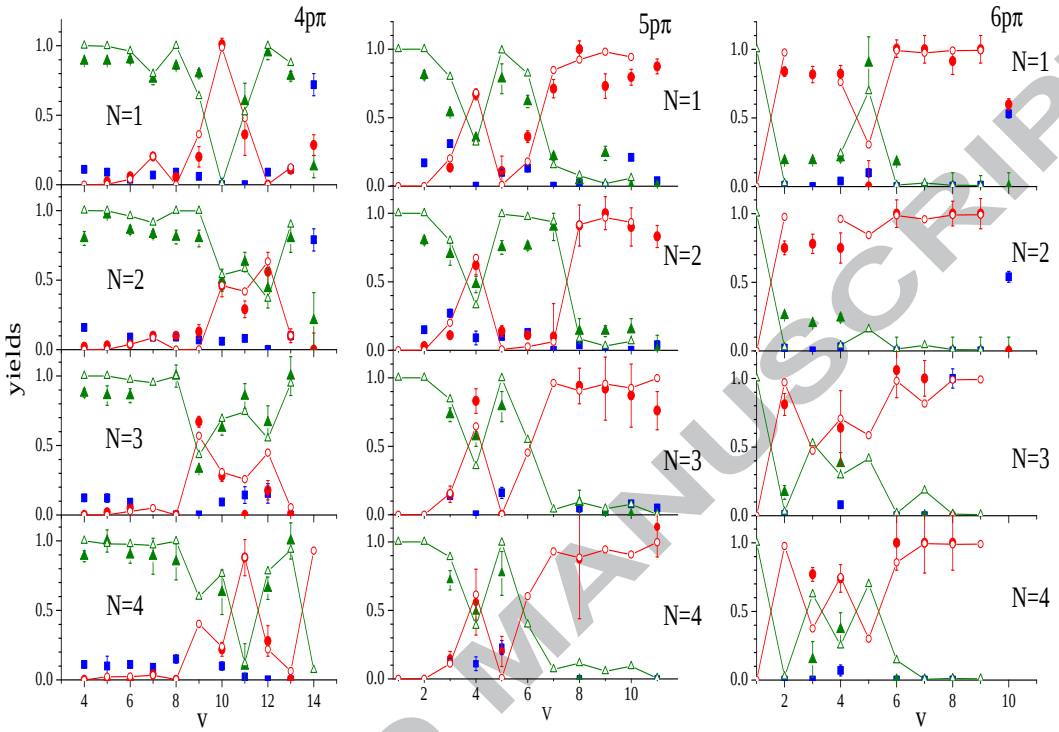

Figure 6.
(Color online) Measured and calculated yield values for the $4p\pi D'$, $5p\pi D''$ and $6p\pi$ $^1\Pi_u^-$ levels of D_2, plotted for various N values as functions of the excited-state vibrational quantum number v. Solid symbols represent measured values (triangles for fluorescence, circles for ionization and squares for dissociation), while for fluorescence (triangles, green online) and ionisation (circles, red online) open symbols connected by lines represent calculated values.

7.4 Branching ratios

While the BESSY experiment does not allow us to directly measure the natural widths of the upper levels of the Q transitions, we have access to the decay dynamics via the branching ratios as determined from Eq. (5). Figure 6 displays the yields for ionization, dissociation and fluorescence for excitation from the ground state to the $np\pi$ states with $n = 4$ (D' state), 5 (D'' state) and 6, respectively. Each figure contains a set of plots for different values of N, and each plot displays the yields as functions the upper state vibrational quantum number. Triangles (green) refer to fluorescence, squares (blue) to dissociation and circles (red) to ionization. The theoretical values are indicated by open symbols connected by lines, whereas filled symbols

(with error bars where appropriate) denote experimental values. No theoretical values are given for some of the highest levels where dissociation into D($n = 3$)+D($n = 1$) becomes possible and may be significant. The reason is that in the absence of a theoretical calculation of this process the branching rations obtained neglecting it are unreliable. Inspection of the three figures demonstrates that the various yields vary strongly as functions of v, with the overall trend being that dissociation is the weakest channel everywhere, and ionization gradually wins over fluorescence as n increases. The figures also show that experiment and theory are, by and large, in agreement, with the strong experimental variations being quite nicely reproduced by theory.

7.4.1 The $4p\pi D'$ upper levels

As we have found previously for H_2, the Q transitions in D_2 leading to the $4p\pi D'$ upper state appear in the fluorescence as well as in the ionization excitation spectrum. A few of them appear also weakly in the dissociation excitation spectrum.

The fluorescence lifetimes of the $4p\pi D'$ state levels calculated by MQDT vary only little with the v and N quantum numbers, that is, they are not significantly affected by local perturbations. These fluorescence lifetimes are of the order of 7.3 ns and turn out to be quite similar to those determined previously for H_2 [18]. Fig. 6 shows that dissociation processes contribute only a few % to the decay of the $4p\pi D'$ state levels. In the MQDT calculations we have neglected this channel as already mentioned (cf. Fig. 6). Note that for $v = 14$ the $4p\pi D'$ state levels are situated above the dissociation limit into D($n = 3$)+D($n = 1$) and may dissociate into this continuum in addition to D($n = 2$)+D($n = 1$).

Despite its weakness predissociation turns out to be more efficient than in H_2 where it has been found to be negligible throughout for $n = 4$ [6]. Two effects are operating here, first, the 'direct' predissociation of the $4p\pi D'$ state to the $2p\pi$ continuum, which must be weaker in D_2 as compared to H_2, and, second, the 'indirect' or 'accidental' predissociation which proceeds via local interaction with levels belonging to the $3p\pi D$ state which in turn are more strongly predissociated. The first of these mechanisms produces mild and smooth variations with v, while the second causes erratic variations to occur. This second effect appears to prevail here, indicating that local perturbations are more widespread in D_2 as compared to H_2, owing to the larger density of levels.

Vibronic autoionization, that is, autoionization occurring through the vibrational coupling to the ionization continua, is expected to scale according to $M^{-1/2}$ [19] so that it should be weaker by a factor $\sqrt{2}$ in D_2 as compared

to H_2. The D_2 $4p\pi D'$ levels can autoionize 'directly' by a $\Delta v < -5$ process, which however is very nearly forbidden and would be exactly zero in the harmonic approximation. Vibrational autoionization may also occur via a local perturbation involving a level that can autoionize by exchange of a single vibrational quantum in a $\Delta v = -1$ process (the only one possible for a harmonic oscillator when the quantum defect varies linearly with R). This 'accidental' autoionization depends not only on the mass, but also sensitively on the energy difference between the interacting levels. Since the D_2 spectrum is much more congested than the H_2 spectrum, the quasi-coincidences are more numerous as our results show.

While we have seen fluorescence to constitute the principal decay channel for the $4p\pi D'$ state levels, a few exceptions should also be noted: (*i*) The level $v = 10, N = 1$ is fully ionized as already mentioned, the reason being that it is mixed with $12p\pi, v = 5, N = 1$ which is rapidly autoionized via a $\Delta v = -1$ interaction. (*ii*) Similarly, the level $v = 11, N = 4$ interacts with $10p\pi, v = 6, N = 4$ which in turn induces rapid autoionization. (*iii*) The transition $Q(4)$ leading to $v = 9, N = 4$ is blended with $Q(2)$ leading to $12p\pi, v = 4, N = 1$ (which is fully ionized) and cannot be fully separated by the present experiment. Based on the measured global yield and the calculated intensities, we estimate the ionization yield of the $4p\pi D', v = 9, N = 4$ level to correspond to 33% in agreement with the theoretical prediction.

7.4.2 The $5p\pi D''$ upper levels

For these levels, fluorescence is an important decay channel, clearly more important than it is for H_2. Experiment and theory agree as shown by Fig. 6. In this case, the mass dependence is as one would intuitively expect: whereas the fluorescence is not mass dependent, the autoionization widths decrease in the heavier isotopomer, thus enhancing the branching fraction into fluorescence.

7.4.3 The $6p\pi$ upper levels

Fluorescence radiation has been detected following the excitation of most of the Q lines leading to the $6p\pi$ state. This is in contrast to H_2 where no such fluorescence has been observed [6]. For $v = 3, N = 1$ and 2, 'complex' resonances occur so that the measured values represent mean yield values. The calculated and measured yields are in good agreement (Fig. 6).

7.4.4 $np\pi$ upper levels with $n \geq 7$

Once the excitation energy exceeds the ionization threshold, decay occurs almost exclusively via the ionization channel. The calculated γ_{ion} values correspond indeed to 100 % to within a few %. The only exceptions are: (*i*) the $7p\pi, v = 2, N = 2$ level for which the measured fluorescence yield is 15 ± 7 %, to be compared with the calculated value of 2%. (*ii*) The $7p\pi, v = 7, N = 1$ level for which a dissociation yield of 17 ± 2 % has been measured. This particular situation may arise from blending with a weak line of a predissociated level (possibly belonging to the $4p\sigma B''$ state).

7.4.5 Summary of analysis of branching ratios

Although the measurement of the natural widths of the $np\pi\,^1\Pi_u^-$ levels of D_2 proved impossible due to the limited energy resolution of the present monochromator experiment, the determination of the fluorescence, dissociation and ionization yields provides detailed information on the partial decay widths, as it has been demonstrated previously for H_2 [6]. As expected, the partial fluorescence widths are roughly the same for D_2 as for H_2. However, this is not the case with regard to the dissociation and ionization partial widths. The ionization widths of the $4p\pi, v, N = 1$ levels observed in H_2 are $\approx 10^{-2}$ cm^{-1}, while for D_2 they are of the order of $\approx 10^{-4}$ cm^{-1} (except for $v = 10$ where the widths are as large as $8 \cdot 10^{-3}$ cm^{-1}). These widths are smaller than in H_2 by more than the expected isotopic factor. On the other hand, the D_2 predissociation widths of the order of $\approx 10^{-4}$ cm^{-1} are still far larger than expected for a direct coupling to the $2p\pi$ continuum.

8 Discussion: Isotope effects

The detailed observations of energy levels, transition intensities and branching ratios presented in the preceding Sections 7.1, 7.2 and 7.4 complement analogous studies carried out previously for H_2 [6, 9, 14]. Taken together with those, they therefore provide extensive material for a discussion of the mass dependence of vibronic coupling in a diatomic molecule. Indeed, the homogeneous $\Pi \sim \Pi$ coupling active within the $^1\Pi_u^-$ $np\pi$ Rydberg manifold and the associated $\epsilon p\pi$ ionization continuum constitutes a paradigmatic example of pure vibronic coupling, not affected by curve crossing nor by non-adiabatic effects associated with rotational motion. In the standard Born-Oppenheimer formulation of non-adiabatic coupling, the main vibronic coupling term has

the familiar form (written here in wavenumber units):

$$H^{(BO)}_{n'v',nv} = -\Big(\frac{h}{2\pi^2 Mc}\Big) < \psi_{n'}|\frac{\partial}{\partial R}|\psi_n >< \chi^{(n')}_{v'}|\frac{\partial}{\partial R}|\chi^{(n)}_{v} > , \qquad (6)$$

where M is the reduced mass, $\psi_n(\mathbf{r}, R)$ and $\chi^{(n)}(R)$ are the electronic and vibrational wavefunction factors in the electronic state n, respectively, with $\mathbf{r}$ and R denoting the electronic coordinates and the bondlength, and where the first factor is an integral over $\mathbf{r}$, while the second factor is an integral over R. $H_{n'v',nv}$ is the interaction matrix element coupling two Born-Oppenheimer levels, n, v and $n'v'$, belonging to two different electronic states. From Eq. (6) it would appear that vibronic coupling has a dependence on nuclear mass that goes as M^{-1}, implying a factor 1/2 between H_2 and D_2. However, the vibrational factor in Eq. (6) is also mass-dependent because the vibrational wavefunctions themselves depend on the nuclear mass. In the harmonic approximation this adds another factor $M^{1/4}$ (see e.g. Appendix III of Ref. [20]) so that the overall dependence of Eq. (6) would go as $\propto M^{-3/4}$, and only matrix elements with $v' = v \pm 1$ differ from zero in this approximation.

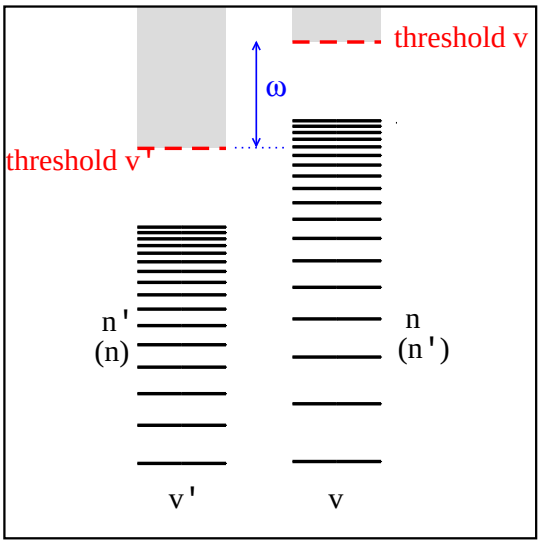

Figure 7.
Interaction between two Rydberg channels (schematic). High levels n associated with the threshold v are embedded in the denser manifold of levels n' associated with v'. Since the vibrational frequency ω [not to be confused with the photon energy occurring in Eqs. (4) and (5)] is mass-dependent, n' and the corresponding level density is also mass-dependent.

The situation changes in high Rydberg states where the motion of the outer electron becomes uncoupled from the vibrational motion. The mass dependence is thereby also modified. It has been shown [19], for instance, that the $\Delta v = -1$ vibrational autoionization of a Rydberg state n, v (a process where a vibrational quantum of energy is converted into electronic energy, allowing the Rydberg electron to escape into the $\epsilon, v-1$ continuum) involves in the harmonic approximation a matrix element which has a $M^{-1/4}$ dependence. In this situation a scattering reaction matrix element must be converted into a Hamiltonian matrix element [21, 22]. Eq. (6) thereby turns into the close-coupling (CC) expression [17]

$$H^{(CC)}_{n'v',nv} = \frac{2Ry}{n'^{3/2}n^{3/2}} \left[\frac{\partial\mu(R)}{\partial R}\right]_{R=R_e} < \chi^{(n')}_{v'}|R-R_e|\chi^{(n)}_{v} > \qquad (7)$$

where Ry is the Rydberg constant and n' and n are the effective principal

quantum numbers of the interacting Rydberg states. μ is the quantum defect and $[\partial\mu(R)/\partial R]_{R=R_e}$ its derivative at R_e with respect to the internuclear distance. Again, in the harmonic approximation only matrix elements with $v' = v \pm 1$ differ from zero. The $M^{-1/4}$ mass dependence stems here from the vibrational factor only. The first factor of Eq. (7) is a Rydberg scaling factor which for $n' = n$ equals the Rydberg level spacing ΔE_{Ryd} in cm^{-1}. The second factor, the quantum defect derivative, measures the strength of the vibronic coupling and is analogous to the electronic factor $< \psi_{n'}|\partial/\partial R|\psi_n >$ in Eq. (6). Knowing that the vibrational frequency ω scales with $M^{-1/2}$ we can conveniently express the above findings in terms of ω as follows:

coupling type	vibronic matrix element
BO	$\propto\ \omega^{\frac{3}{2}}$
CC	$\propto\ \omega^{\frac{1}{2}}$.

Local interactions depend on the magnitude of the vibronic channel interaction, but also on the density of interacting levels n' available to participate in interchannel coupling and local perturbations. Fig. 7 illustrates this for two Rydberg channels whose thresholds are separated by the vibrational frequency ω. We first examine the situation where a Rydberg level n, v interacts with n', v', where v' is smaller than v. For given n, n' is trivially obtained via the Rydberg relation $Ry/n^2 = Ry/n'^2 + \omega$ (see the figure). Having determined n' we can evaluate the level density $1/\Delta E_{Ryd} = n'^3/(2Ry)$ and the matrix element $H^{(CC)}_{n'v',nv}$ according to Eq. 7. The significant quantity here appears to be the effective coupling strength $H/\Delta E$ which, for given n and ω, is found to scale according to

$$\frac{H^{(CC)}}{\Delta E_{Ryd}} \quad \text{effective coupling strength} \quad \propto \frac{\omega^{\frac{1}{2}}}{[1 \mp n^2(\omega/Ry)]^{\frac{3}{4}}}\ , \quad (\mp \text{ for } v' \lesseqgtr v,\ n' \gtreqless n). \tag{8}$$

We may also envision the situation where a Rydberg level n, v interacts with n', v' where v' is larger than v and consequently n' is smaller than n. In this event the labels n and n' in brackets in Fig. 7 have to be considered and the same expression (8) is obtained with a + sign instead of a − sign in the denominator. The effective coupling strengths have been evaluated with Eq. (8) by use of the vibrational frequencies ω_e for H_2^+ (2321 cm^{-1}) and D_2^+ (1577 cm^{-1}), the appropriate values of the Rydberg constant, and setting the value for H_2 to unity for the purposes of comparison. The results are:

		effective coupling strength $H^{(CC)}_{n'v',nv}/\Delta E_{Ryd}$	
		H_2	D_2
$v' < v,\ n' > n$	$n = 4$	1.00	0.74
	$n = 5$	1.00	0.65
	$n = 6$	1.00	0.49
$v' > v,\ n' < n$	$n = 4$	1.00	0.88
	$n = 5$	1.00	0.90
	$n = 6$	1.00	0.92

These numbers indicate that under the assumptions made here, the effective coupling strength should always be weaker in D_2 than in H_2 when $v' < v$ (Fig. 7), and there should be almost no isotope effect when $v' > v$. This is in apparent contradiction to what we have established experimentally and reproduced by the multichannel quantum defect calculations, as detailed in the preceding Sections.

The outcome of this discussion then is that the occurrence of small local perturbations, which is more widespread in D_2 as compared to H_2 despite the fact that the vibronic interactions are intrinsically weaker in the heavier isotopomer, must be a genuine *multichannel effect* - and as such is accounted for by MQDT - but cannot be understood with the help of the two-channel picture of Fig. 7. The intuitive expectation that the level structure is denser in the heavier isotope, and more local perturbations can therefore occur, appears to be correct, but requires a *large number* of interacting vibrational channels in order to become operative.

9 Conclusion

We have measured the absolute transition probabilities of 319 $Q(N)$ photoabsorption transitions ${}^1\Pi_u^-, v, N \leftarrow X, v'' = 0, N''$ in D_2. 143 new $Q(N)$ lines have been identified and assigned. The observations have been interpreted theoretically by MQDT under the assumption that excited electronic states are correctly described as $np\pi$ Rydberg states associated with the vibrating/rotating (v^+, N^+) ground state ion. It has been known for a long time that these levels exhibit strong non-adiabatic coupling in H_2; here we have extended the previous analyses and studied the effect of the interactions on the line intensities. In this paper, we presented detailed evidence for slow decay processes active in numerous superexcited molecular levels of D_2. These processes take place typically on the sub-μs scale but remain slower than 1 ns. Due to our absolute absorption and partial decay cross section measurements, we have been able to characterize these slow processes in detail, despite the

fact that the corresponding natural widths of the excited states studied here are by orders of magnitude smaller than our experimental spectral resolution which is limited by the Doppler width. The theoretical approach [9] implemented in this work fully accounts for the observed dynamics and includes autoionization and spontaneous photon emission. While our theoretical approach as such is not new and has been shown previously to be a powerful tool for the description of many aspects of the internal dynamics of molecular hydrogen (see, e.g., various papers collected in Ref. [26]), it is applied here in an unprecedented systematic way. It appears that MQDT is capable of describing the various very weak couplings quite accurately, involving both vibronic interaction and radiative decay. The observation and characterization of spontaneous photon emission in a large number of superexcited levels constitutes a remarkable exception in the field of molecular physics because in general in small molecules predissociation and autoionization processes completely quench molecular fluorescence once they are energetically possible.

10 Acknowledgments

We acknowledge the Helmholtz-Zentrum Berlin electron storage ring BESSY II for provision of synchrotron radiation at beam line U125/2-10m-NIM. The research leading to these results has received funding from the European Community Seventh Framework Programme (FP7/2007-2013) under Grant No. 226716, and it has been supported by the State Initiative for the Development of Scientific and Economic Excellence (LOEWE) in the LOEWE-Focus ELCH and by the German Federal Ministry of Education and Research (BMBF, Project: 0K13RK1). Ch. J. thanks the Miescher Foundation (Basel, Switzerland) for partial support. Ch. J. was further supported by the ANR (France) under Contract 09-BLAN-020901.

References

[1] M. Glass-Maujean, Ch. Jungen, M. Roudjane and W.-Ü. L. Tchang-Brillet, J. Chem. Phys. **134**, 204305-1 - 204305-14 (2011).

[2] L. Wolniewicz and G. Staszewska, J. Mol. Spectrosc. **220**, 45-51 (2003).

[3] http://fizyka.umk.pl/ftp/pub/publications/ifiz/luwo .

[4] M. Glass-Maujean, Ch. Jungen, G. D. Dickenson, W. Ubachs, N. de Oliveira, D. Joyeux, and L. Nahon, J. Mol. Spectrosc. (preceding paper).

[5] M. Bacal, M. Glass-Maujean, A. A. Ivanov, M. M. Nishiura, M. Sasao, and M. Wada , in: *Production and Neutralization of Negative Ions and Beams*, ed. M. P. Stockli, AIP Conf. Proceedings **639**, 13-20 (2002).

[6] M. Glass-Maujean, Ch. Jungen, G. Reichardt, A. Balzer, H. Schmoranzer, A. Ehresmann, I. Haar, and P. Reiss, Phys. Rev. **A 82**, 062511-1 - 062511-13 (2010).

[7] M. Glass-Maujean, S. Klumpp, L. Werner, A. Ehresmann, H. Schmoranzer, Mol. Phys. **105**, 1535-1542 (2007).

[8] G. Reichardt, J. Bahrdt, J.-S. Schmidt, W. Gudat, A. Ehresmann, R. Müller-Albrecht, H. Molter, H. Schmoranzer, M. Martins, N. Schwentner and S. Sasaki, Nucl. Instrum. Methods Phys. Res. Sect. A **467-468**, 462-465 (2001).

[9] M. Glass-Maujean and Ch. Jungen, J. Phys. Chem. **A113**, 13124-13132 (2009).

[10] G. D. Dickenson, T. I. Ivanov, W. Ubachs, M. Roudjane, N. de Oliveira, D. Joyeux, L. Nahon, W.-Ü. L. Tchang-Brillet, M. Glass-Maujean, H. Schmoranzer, A. Knie, S. Kübler, and A. Ehresmann, Mol. Phys. **109**, 2693-2708 (2011).

[11] S. Takezawa and Y. Tanaka, J. Mol. Spectrosc. **54**, 379-401 (1975).

[12] R. S. Freund, J. A. Schiavone, and H. M. Crosswhite, J. Phys. Chem. Ref. Data **14**, 235-283 (1985).

[13] M. Roudjane, F. Launay, and W.-Ü. L. Tchang-Brillet, J. Chem. Phys. **125**, 214305-1 - 214305-9 (2006).

[14] M. Glass-Maujean, Ch. Jungen, A. Spielfiedel, and H. Schmoranzer, J. Mol. Spectrosc. **293-294**, 1-10 (2013).

[15] M. Glass-Maujean, S. Klumpp, L. Werner, A. Ehresmann, and H. Schmoranzer, J. Chem. Phys. **128**, 094312-1 - 094312-9 (2008).

[16] M. Glass-Maujean, Ch. Jungen, H. Schmoranzer, I. Tulin, A. Knie, P. Reiss, and A. Ehresmann, J. Mol. Spectrosc. **293-294**, 11-18 (2013).

[17] G. Herzberg and Ch. Jungen, J. Mol. Spectrosc. **41**, 425-486 (1972).

[18] M. Glass-Maujean, J. Breton, B. Thièblemont, K. Ito, J. Physique **45**, 1107-1111 (1984).

[19] S. T. Pratt and Ch. Jungen, J. Chem. Phys. **137**, 174306-1 - 174306-6 (2012).

[20] E. B. Wilson, J. C. Decius, and P. C. Cross, *Molecular Vibrations*, (McGraw-Hill, New York, 1955), Appendix III.

[21] A. Giusti-Suzor and Ch. Jungen, J. Chem. Phys. **80**, 986-1000 (1984).

[22] S. Fredin, D. Gauyacq, M. Horani, Ch. Jungen, G. Lefevre, and F. Masnou-Seeuws, Mol. Phys. **60**, 825-866 (1987).

[23] M. Glass-Maujean, Ch. Jungen, H. Schmoranzer, I. Tulin, A. Knie, P. Reiss, and A. Ehresmann, J. Mol. Spectrosc. **293-294**, 19-26 (2013).

[24] J. Liu, D. Sprecher, Ch. Jungen, W. Ubachs, and F. Merkt, J. Chem. Phys. **132**, 154301-1 - 154301-11 (2010).

[25] H. Bredohl and G. Herzberg, Can. J. Phys. **51**, 867-887 (1973).

[26] *Molecular Applications of Quantum Defect Theory*, ed. Ch. Jungen (Institute of Physics, Bristol, 1996).

Table 1. $Q(1)$ transitions in the photoabsorption spectrum of the D_2 molecule

	v	$Q(1)$ (obs) [a]	$obs-calc$	A_{calc} [b]	A_{obs}	γ_{diss} [c]	γ_{fluo}	γ_{ion}
$5p\pi$	2	123564.8[d]	-0.1	9.93	11.4 ± 1.7	17 ± 1	81 ± 3	
$10p\pi$	0	123635.5	0.1	0.33	0.4 ± 0.1	0 ± 9	84 ± 16	
$11p\pi$	0	123821.5	0.0	0.28	0.4 ± 0.5	0 ± 8	79 ± 21	
$13p\pi$	0	124074.2	0.5	0.27	[e]			
$4p\pi$	4	124090.4	-0.3	24.03	19.9 ± 2.5	11 ± 1	89 ± 2	
$7p\pi$	1	124104.3	-0.8	2.00	[e]			
$16p\pi$	0	124290.9	0.1	0.09	0.2 ± 0.1	28 ± 5	72 ± 5	
$17p\pi$	0	124338.8	-0.2	0.08	0.1 ± 0.1	0 ± 21	100 ± 21	
$8p\pi$	1	124612.0	-0.1	1.98	5.0 ± 0.9	61 ± 3	20 ± 2	19 ± 5
$6p\pi$	2	124839.9	-0.3	7.88	8.1 ± 1.2	1 ± 0	18 ± 1	81 ± 3
$9p\pi$	1	124961.7	0.0	1.14	[e]			
$5p\pi$	3	125018.9	0.1	10.64	14.6 ± 2.3	32 ± 1	54 ± 2	14 ± 1
$10p\pi$	1	125212.1	0.0	0.89	[e]			
$11p\pi$	1	125397.5	-0.5	0.75	0.8 ± 0.2	0 ± 2	0 ± 8	100 ± 13
$4p\pi$	5	125425.4	-0.2	18.90	17.4 ± 3.4	9 ± 1	89 ± 5	2 ± 0
$12p\pi$	1	125539.9	0.3	0.65	2.2 ± 0.6	0 ± 1	0 ± 5	100 ± 6
$7p\pi$	2	125617.7	-0.3	3.94	7.2 ± 1.1	1 ± 0	6 ± 1	93 ± 1
$15p\pi$	1	125809.1	0.2	0.27	0.8 ± 0.2	5 ± 1	0 ± 7	95 ± 8

[a] observed transition energy, in cm^{-1}.

[b] A, emission probability for the transition to $X^1\Sigma_g^+, v''=0, N''=N$, in 10^6 s^{-1}.

[c] γ, experimental decay branching ratio in %.

[d] The positions of the upper state energy levels above the $v''=0, N''=0$ ground state level are obtained by adding the ground-state rotational energy 59.78 cm^{-1} ($N''=1$) [24] to the transition energy.

[e] Blended line

[f] Transition energies in boldface correspond to new assignments.

[g] A coefficients in italics correspond to the sum of the calculated intensities to a group of interacting upper levels.

) Double assignment to Q transitions (blended line). The observed intensity corresponds to the sum of the two transitions.

* Dissociation into D($n=3$)+D($n=1$).

Table 1 (continued)

	v	$Q(1)$ (obs) [a]	$obs-calc$	A_{calc} [b]	A_{obs}	γ_{diss} [c]	γ_{fluo}	γ_{ion}
$16p\pi$	1	125867.3	0.4	0.23	0.3 ± 0.2	0 ± 4	0 ± 20	100 ± 24
$8p\pi$	2	126123.8	-0.6	3.14	9.6 ± 1.2	2 ± 0	13 ± 1	85 ± 1
$6p\pi$	3	126290.6	0.2	*9.35*[g]	10.8 ± 1.6	0 ± 1	19 ± 1	81 ± 1
$5p\pi$	4	126411.2	0.1	9.51	12.2 ± 2.2	0 ± 1	34 ± 3	66 ± 4
$9p\pi$	2	126473.3	-0.7	1.49	5.1 ± 1.6	12 ± 2	30 ± 4	58 ± 6
$4p\pi$	6	126701.0	0.1	15.49	12.0 ± 2.7	4 ± 2	89 ± 7	6 ± 8
$11p\pi$	2	126909.4	-0.4	1.12	1.0 ± 0.7	17 ± 7	0 ± 29	83 ± 37
$12p\pi$	2	127050.5	-0.2	1.64	1.9 ± 0.3	0 ± 1		100
$7p\pi$	3	127068.8	-0.1	3.65	3.6 ± 1.2	0 ± 1		100
$13p\pi$	2	127162.0	0.1	0.54	0.4 ± 0.1	0 ± 3		100
$14p\pi$	2	127249.0	-0.5	0.49	[e]			100
$15p\pi$	2	127319.7	-0.6	0.42	0.5 ± 0.4			100
$8p\pi$	3	127573.4	0.2	4.20	5.0 ± 1.2	0 ± 0	0 ± 2	100
$6p\pi$	4	127677.0	-0.2	11.17	9.2 ± 1.5	3 ± 0	19 ± 3	77 ± 3
$5p\pi$	5	127744.6	0.0	6.17	6.1 ± 1.8	10 ± 2	74 ± 8	17 ± 10
$4p\pi$	7	127917.3	0.0	11.24	11.5 ± 2.1	7 ± 0	75 ± 2	19 ± 3
$9p\pi$	3	127922.3	-0.7	1.72	4.3 ± 1.8	0 ± 1		100 ± 1
$10p\pi$	3	128172.8	-0.1	1.56	1.5 ± 0.9	0 ± 1	0 ± 8	100 ± 9
$11p\pi$	3	128357.9	-0.5	1.36	1.5 ± 0.3	0 ± 0	0 ± 8	100 ± 9
$7p\pi$	4	128456.1	-0.3	4.56	4.6 ± 1.1	0 ± 0	4 ± 1	96 ± 1
$12p\pi$	3	128499.6	-0.7	0.60	0.6 ± 0.2	0 ± 2	0 ± 10	100 ± 12
$13p\pi$	3	128611.7	1.3	0.67	1.5 ± 0.6	0 ± 2	0 ± 4	100 ± 6
$15p\pi$	3	128768.6	-0.2	0.50	0.5 ± 0.4	0 ± 2	0 ± 11	100 ± 13
$18p\pi$	3	128915.7	0.4	0.41	0.4 ± 0.5	0 ± 3	0 ± 14	100 ± 17
$19p\pi$	3	128949.5	0.2	0.91	0.7 ± 0.2	0 ± 2	0 ± 9	100 ± 11
$8p\pi$	4	128959.9	0.6	7.22	9.0 ± 2.5	6 ± 1	34 ± 2	60 ± 2
$5p\pi$	6	128993.1	0.7	12.53	15.8 ± 3.5	12 ± 1	56 ± 2	33 ± 3
$6p\pi$	5	129029.9	0.4	0.41	0.3 ± 0.3	9 ± 3	91 ± 21	0 ± 24
$4p\pi$	8	129077.4	0.2	6.33	5.2 ± 0.7	9 ± 1	86 ± 3	5 ± 4
$9p\pi$	4	129310.8	0.3	1.89	2.2 ± 1.1	0 ± 1	0 ± 3	100 ± 4

Table 1 (continued)

	v	$Q(1)$ (obs) [a]	$obs-calc$	A_{calc} [b]	A_{obs}	γ_{diss} [c]	γ_{fluo}	γ_{ion}
$10p\pi$	4	129560.5	0.3	1.56	4.5 ± 0.8	0.0 ± 0.3	0 ± 2	100 ± 2
$11p\pi$	4	129744.5	-0.6	1.67	2.0 ± 0.4	0 ± 1	0 ± 3	100 ± 4
$7p\pi$	5	129784.3	-0.7	3.52	5.0 ± 1.8	18 ± 2	0 ± 1	82 ± 3
$13p\pi$	4	129997.2	-0.2	0.69	0.6 ± 0.3	0 ± 6	0 ± 10	100 ± 16
$14p\pi$	4	130084.6	-0.4	0.61	5.3 ± 0.9	4 ± 1	15 ± 2	81 ± 2
$15p\pi$	4	130155.3	-0.4	0.67	1.0 ± 0.6	0 ± 1	0 ± 6	100 ± 8
$4p\pi$	9	130168.6	0.4	12.15	10.7 ± 1.5	6 ± 1	75 ± 2	19 ± 3
$16p\pi$	4	130213.0	-0.6	0.72	1.1 ± 0.4	0 ± 1	0 ± 12	100 ± 13
$5p\pi$	7	130222.3	-0.1	4.57	5.8 ± 1.6	0 ± 1	23 ± 2	77 ± 3
$6p\pi$	6	130280.4	-0.3	3.39	11.0 ± 2.4	0 ± 1	15 ± 2	85 ± 2
$19p\pi$	4	**130336.7**[f]	0.2	0.16	0.2 ± 0.3	0 ± 6		100 ± 6
$20p\pi$	4	**130365.6**	-0.1	0.16	0.2 ± 0.1	0 ± 8		100 ± 8
$22p\pi$	4	**130412.4**	-0.3	0.13	0.2 ± 0.3			100
$23p\pi$	4	**130431.2**	-0.4	0.12	[e]			100
$26p\pi$	4	**130476.3**	0.0	0.08	0.1 ± 0.1			100
$27p\pi$	4	**130488.8**	0.8	0.08	0.2 ± 0.1			100
$28p\pi$	4	**130498.5**	0.1	0.07	0.2 ± 0.3			100
$9p\pi$	5	130637.4	-0.3	1.71	2.0 ± 0.4			100
$10p\pi$	5	130886.5	-0.7	1.43	1.7 ± 0.5			100
$7p\pi$	6	131052.2	0.2	4.05	3.5 ± 1.6			100
$4p\pi$	10	131213.2	-0.6	4.41)	7.6 ± 1.1		0 ± 2	100 ± 2
$12p\pi$	5	131213.2	-1.1	2.77)				
$13p\pi$	5	131323.6	-0.4	0.67	0.7 ± 0.4	0 ± 2		100 ± 2
$5p\pi$	8	131376.6	-0.2	5.06	4.7 ± 2.1	2 ± 1	3 ± 5	95 ± 5
$14p\pi$	5	131410.7	-0.9	0.46	[e]	0 ± 1	0 ± 8	100 ± 9
$15p\pi$	5	131481.5	-0.6	0.73	0.8 ± 0.4	0 ± 2		100 ± 2
$6p\pi$	7	131494.6	0.4	2.65	3.3 ± 1.2		0 ± 4	100 ± 4
$8p\pi$	6	131559.1	-0.4	1.21	1.6 ± 0.7	0 ± 1		100 ± 1
$18p\pi$	5	**131628.8**	0.0	0.19	0.3 ± 0.4			100
$20p\pi$	5	**131692.5**	0.3	0.15	0.3 ± 0.2			100

Table 1 (continued)

	v	$Q(1)$ (obs) [a]	$obs-calc$	A_{calc} [b]	A_{obs}	γ_{diss} [c]	γ_{fluo}	γ_{ion}
$43p\pi$	5	131904.9	0.3	0.35	[e]	0	0	100
$9p\pi$	6	131904.9	-0.8	1.04		3±1	0 ± 4	97 ± 5
$10p\pi$	6	132154.9	0.1	1.31	1.2 ± 0.6	0 ± 1	0 ± 10	100 ± 11
$4p\pi$	11	132199.0	-0.8	4.41	5.6 ± 3.8	13 ± 3	53 ± 3	34 ± 6
$7p\pi$	7	132263.1	-0.2	2.52	2.9 ± 0.6	6 ± 2	25 ± 24	69 ± 26
$11p\pi$	6	132340.7	0.1	0.67	0.5 ± 0.3	0 ± 2	0 ± 22	100 ± 22
$5p\pi$	9	132474.8	0.1	4.08	5.2 ± 1.4	0 ± 1	25 ± 5	75 ± 6
$13p\pi$	6	132591.9	0.4	0.55	2.2 ± 0.8	0 ± 1	0 ± 6	100 ± 7
$6p\pi$	8	132647.9	0.9	2.45	3.3 ± 1.0	0 ± 1	0 ± 4	100 ± 5
$15p\pi$	6	132748.9	-0.7	0.45	2.2 ± 0.8	5 ± 1	54 ± 6	40 ± 6
$8p\pi$	7	132769.0	0.1	1.15	1.1 ± 0.3			100
$16p\pi$	6	**132807.8**	-0.1	0.19	0.3 ± 0.3			100
$9p\pi$	7	133115.0	-0.2	1.25	1.4 ± 0.5	4 ± 1	0 ± 9	96 ± 10
$4p\pi$	12	133126.8	-0.9	2.80	4.1 ± 1.1	8 ± 1	92 ± 6	0 ± 2
$10p\pi$	7	133364.0	0.0	1.19	1.6 ± 0.7	0 ± 1	0 ± 8	100 ± 8
$7p\pi$	8	133414.9	-1.3	2.02	1.9 ± 0.4	0 ± 1	0 ± 7	100 ± 8
$5p\pi$	10	133516.5	0.3	2.51	3.8 ± 0.8	21 ± 1	0 ± 3	79 ± 2
$11p\pi$	7	133550.0	0.1	0.50	0.4 ± 0.1			100
$12p\pi$	7	133690.0	-0.8	0.56	[e]		0	
$6p\pi$	9	133744.0	0.9	1.86	1.6 ± 0.6	1 ± 1	0 ± 8	99 ± 2
$14p\pi$	7	133888.5	0.3	0.38	[e]			
$4p\pi$	13	133994.5	-3.2	2.01	1.9 ± 0.8	10 ± 2	79 ± 8	10 ± 2
$24p\pi$	7	134265.5	-0.1	0.43	0.6 ± 0.2	4 ± 2	0	96 ± 2
$9p\pi$	8	134268.2	0.2	0.54	0.5 ± 0.2	7 ± 3	0	93 ± 2
$5p\pi$	11	134492.9	-0.9	3.88	4.1 ± 0.9	4 ± 0	0	96 ± 2
$6p\pi$	10	134783.2	0.9	1.67	1.6 ± 0.2	47 ± 2*		53 ± 2
$4p\pi$	14	134805.9	-4.0	1.09	1.7 ± 0.6	64 ± 7*	11 ± 8	25 ± 2
$12p\pi$	8	**134842.6**	-0.4	0.31	1.4 ± 0.3			
$5p\pi$	12	135426.0	0.5	1.76		77 ± 4*		23 ± 4
$52p\pi$	8	135555.8	4.1	0.23)				
$7p\pi$	10	135555.8	3.5	0.74)	1.4 ± 0.2			
$4p\pi$	15	135564.0	0.7	0.77	0.6 ± 0.1	100*		
$4p\pi$	16	136252.4	1.5	1.43	1.1 ± 0.2	100*		
$4p\pi$	17	**136887.3**	0.5	0.65	0.7 ± 0.1	100*		

Table 2. Same as Table 1 for the $Q(2)$ transitions

	v	$Q(2)$ (obs) [a]	$obs-calc$	A_{calc} [b]	A_{obs}	γ_{diss} [c]	γ_{fluo}	γ_{ion}
$5p\pi$	2	123500.2[d]	0.1	9.94	10.3 ± 1.3	16 ± 2	84 ± 2	
$10p\pi$	0	123575.0	0.2	0.33	0.35 ± 0.07	28 ± 9	72 ± 9	
$11p\pi$	0	123760.6	-0.2	0.28	0.4 ± 0.1	15 ± 6	85 ± 6	
$12p\pi$	0	123902.2	-0.3	0.24	0.6 ± 0.3	0 ± 17	99 ± 17	
$13p\pi$	0	124013.0	0.0	0.30	[e]			
$4p\pi$	4	124021.8	0.0	23.91	23 ± 4	16 ± 1	84 ± 1	
$7p\pi$	1	124042.4	0.2	2.15	2.0 ± 0.3	50 ± 8	50 ± 8	
$8p\pi$	1	124548.7	-0.6	1.83	[e]	24 ± 2	76 ± 2	
$6p\pi$	2	124774.8	-0.5	7.89	8.4 ± 1.1	2 ± 1	26 ± 3	72 ± 3
$9p\pi$	1	**124899.8**[f]	1.0	1.15	[e]			
$5p\pi$	3	124949.7	-2.1	10.61	4.9 ± 1.0	24 ± 5	66 ± 8	10 ± 3
$10p\pi$	1	125148.9	-0.3	0.89	0.9 ± 0.3	0 ± 5	0 ± 19	100 ± 24
$11p\pi$	1	125334.2	-0.9	0.76	[e]			
$4p\pi$	5	125354.7	-0.1	18.90	14 ± 3	0 ± 1	97 ± 2	3 ± 1
$12p\pi$	1	**125476.9**	0.2	0.65	[e]			
$7p\pi$	2	125553.0	-0.1	3.93	4.3 ± 1.0	1 ± 1	9 ± 4	90 ± 5
$13p\pi$	1	**125587.0**	-0.5	0.26	0.4 ± 0.2	0 ± 10		100 ± 10
$14p\pi$	1	125674.8	-0.3	0.31	[e]			
$15p\pi$	1	125746.1	0.2	0.27	0.3 ± 0.3			100
$17p\pi$	1	125852.4	0.1	0.20	0.3 ± 0.1			100
$18p\pi$	1	**125893.5**	0.8	0.17	0.3 ± 0.1			
$8p\pi$	2	126059.8	0.3	3.07	3.4 ± 0.5	2 ± 1	16 ± 3	82 ± 4
$6p\pi$	3	126223.4	0.1	*9.59*[g]	10.0 ± 1.5	0 ± 1	20 ± 3	80 ± 3
$5p\pi$	4	126342.3	0.1	9.45	8.2 ± 1.8	8 ± 4	40 ± 9	52 ± 4
$9p\pi$	2	126410.6	1.7	1.51	[e]			
$4p\pi$	6	126627.5	-0.5	15.34	13 ± 2	9 ± 2	86 ± 14	4 ± 1
$10p\pi$	2	126658.5	-0.6	1.32	1.2 ± 0.3	0 ± 4		100 ± 4

[a] observed transition energy, in cm^{-1}.

[b] A, emission probability for the transition to $X^1\Sigma_g^+, v''=0, N''=N$, in 10^6 s^{-1}.

[c] γ, experimental decay branching ratio in %.

[d] The positions of the upper state energy levels above the $v''=0, N''=0$ ground state level are obtained by adding the ground-state rotational energy 179.01 cm^{-1} ($N''=2$) [25] to the transition energy.

[e] Blended line

[f] Transition energies in boldface correspond to new assignments.

[g] A values in italics correspond to the sum of the calculated intensities to a group of interacting upper levels.

) Double assignment to Q transitions (blended line). The observed intensity corresponds to the sum of the two transitions.

* Dissociation into D($n=3$)+D($n=1$).

Table 2 (continued)

	v	$Q(2)$ (obs) [a]	$obs-calc$	A_{calc} [b]	A_{obs}	γ_{diss} [c]	γ_{fluo}	γ_{ion}
$11p\pi$	2	126844.1	-0.6	1.12	[e]			
$12p\pi$	2	126985.9	0.3	1.75	1.1 ± 0.4	0 ± 4		100 ± 4
$7p\pi$	3	127001.9	0.0	3.53	4.6 ± 0.6	0 ± 1		100 ± 1
$13p\pi$	2	127095.4	-1.5	0.55	[e]			
$14p\pi$	2	127184.8	0.3	0.49	0.3 ± 0.1			100
$15p\pi$	2	127255.4	0.1	0.42	0.2 ± 0.2			100
$8p\pi$	3	127506.5	0.2	4.22	3.7 ± 0.6			100 ± 4
$6p\pi$	4	127607.8	-0.3	8.30	10.8 ± 2.0	3 ± 1	23 ± 5	74 ± 5
$5p\pi$	5	127673.9	0.2	6.06	7.6 ± 1.1	10 ± 2	77 ± 13	13 ± 4
$4p\pi$	7	127842.3	-0.3	11.15	9.6 ± 1.6	9 ± 2	81 ± 14	10 ± 2
$9p\pi$	3	127855.4	-0.5	1.81	1.7 ± 0.2			100
$10p\pi$	3	128105.8	-0.1	1.56	[e]			
$11p\pi$	3	128290.4	-0.9	1.37	[e]			
$7p\pi$	4	128387.4	0.1	4.54	4.7 ± 0.9	0 ± 1	0 ± 10	100 ± 10
$12p\pi$	3	**128433.9**	0.6	0.62	[e]	0	0	100
$13p\pi$	3	**128543.2**	-0.1	0.67	0.7 ± 0.1	0	0	100
$14p\pi$	3	**128631.2**	0.3	0.58	0.5 ± 0.1	0 ± 10	0 ± 10	100 ± 10
$16p\pi$	3	**128760.1**	0.4	0.44	0.5 ± 0.2	0	0	100
$19p\pi$	3	128882.3	0.1	1.20	0.9 ± 0.3	0	0	100
$8p\pi$	4	128890.3	0.2	7.43	8.7 ± 1.7	0	0	100
$5p\pi$	6	128921.1	0.7	12.23	11.4 ± 1.6	12 ± 2	77 ± 3	11 ± 2
$6p\pi$	5	**128959.1**	1.6	0.25	[e]			
$4p\pi$	8	129000.9	0.2	6.21	5.5 ± 1.2	7 ± 2	85 ± 5	8 ± 2
$9p\pi$	4	129241.7	0.3	1.89	1.8 ± 0.6			100
$10p\pi$	4	129491.0	-0.1	1.56	1.7 ± 0.3			100
$11p\pi$	4	129675.8	-0.2	1.70	1.7 ± 0.3			100
$7p\pi$	5	129713.1	-0.8	3.48	3.2 ± 0.4			100
$13p\pi$	4	129928.1	-0.1	0.69	0.9 ± 0.2			100
$4p\pi$	9	130091.0	1.0	11.41	11.2 ± 2.0	8 ± 2	77 ± 7	14 ± 6
$5p\pi$	7	130147.3	-0.1	3.99	2.9 ± 1.2	0 ± 2	92 ± 20	8 ± 18

Table 2 (continued)

	v	$Q(2)$ (obs) [a]	$obs-calc$	A_{calc} [b]	A_{obs}	γ_{diss} [c]	γ_{fluo}	γ_{ion}
$6p\pi$	6	130207.5	-0.7	3.37	3.7 ± 1.8			100
$9p\pi$	5	130566.3	-0.5	1.16	1.7 ± 0.4			100
$10p\pi$	5	130815.3	-0.7	1.44	1.6 ± 0.4			100
$7p\pi$	6	130978.7	-0.4	4.01	4.0 ± 0.6			100
$4p\pi$	10	131133.2	-0.4	6.53	6.7 ± 1.1	5 ± 1	51 ± 9	43 ± 9
$12p\pi$	5	**131142.5**	-0.3	0.64	0.5 ± 0.3			100
$13p\pi$	5	**131252.9**	0.0	0.68	[e]			
$5p\pi$	8	131299.8	-0.2	5.05	5.7 ± 0.8	4 ± 2	13 ± 8	84 ± 10
$15p\pi$	5	**131410.7**	-0.2	0.90	0.8 ± 0.1			100
$6p\pi$	7	131419.4	0.1	2.48	[e]			
$16p\pi$	5	**131468.6**	-0.4	0.41	0.4 ± 0.2			100
$8p\pi$	6	131485.8	-0.7	1.20	1.5 ± 0.4			100
$9p\pi$	6	131832.5	0.1	1.20	1.3 ± 0.4			100
$10p\pi$	6	132081.7	0.0	1.32	1.2 ± 0.3			100
$4p\pi$	11	132116.9	-0.4	4.36	4.5 ± 0.9	8 ± 1	65 ± 8	28 ± 7
$7p\pi$	7	132188.1	-0.2	2.54	2.3 ± 0.6			100
$11p\pi$	6	**132267.3**	-0.2	0.68	0.6 ± 0.4			100
$5p\pi$	9	132396.6	0.5	3.93	3.5 ± 0.6	0 ± 1	12±4	88 ± 6
$13p\pi$	6	**132518.6**	0.2	0.56	0.5 ± 0.2			100
$6p\pi$	8	132568.7	-1.4	2.43	2.6 ± 0.4			100
$14p\pi$	6	**132606.1**	0.1	0.32	0.3 ± 0.1			100
$15p\pi$	6	**132676.6**	0.2	0.47	0.3 ± 0.1			100
$8p\pi$	7	132693.9	-0.1	1.13	1.1 ± 0.3			100
$9p\pi$	7	133040.6	0.4	1.64	2.6 ± 0.6			100
$4p\pi$	12	133042.7	-0.5	2.33	2.1 ± 0.4	0 ± 2	46 ± 17	54 ± 19
$10p\pi$	7	133287.8	-1.2	1.20	[e]			100
$7p\pi$	8	133338.9	-0.4	2.02	2.2 ± 0.4			100
$5p\pi$	10	133435.7	0.1	2.48	2.3 ± 0.6	0 ± 2	15 ± 8	85 ± 10
$11p\pi$	7	**133474.9**	0.0	0.52	0.7 ± 0.2			100
$12p\pi$	7	**133616.1**	0.3	0.57	0.8 ± 0.2			100

Table 2 (continued)

	v	$Q(2)$ (obs) [a]	$obs-calc$	A_{calc} [b]	A_{obs}	γ_{diss} [c]	γ_{fluo}	γ_{ion}
$6p\pi$	9	133660.3	-4.0	1.85	1.8 ± 0.3			100
$13p\pi$	7	**133726.0**	0.1	0.34	0.2 ± 0.1			100
$14p\pi$	7	**133813.1**	-0.1	0.39	0.6 ± 0.5			100
$8p\pi$	8	133844.1	0.0	1.04	1.1 ± 0.2			100
$4p\pi$	13	133907.8	-3.4	2.01	2.0 ± 0.4	8 ± 2	84 ± 6	8 ± 4
$25p\pi$	7	**134190.1**	0.2	0.81)	1.2 ± 0.2			100
$9p\pi$	8	134190.1	-1.8	0.15)				
$5p\pi$	11	134412.1	0.0	3.71	3.9 ± 0.5	5 ± 3	0 ± 11	95 ± 11
$7p\pi$	9	**134434.1**	-0.6	0.46	0.5 ± 0.1	7 ± 4	0 ± 22	93 ± 22
$11p\pi$	8	**134623.9**	-1.0	0.51	[e]			
$6p\pi$	10	134705.2	3.7	1.81	1.8 ± 0.4	54 ± 4	46 ± 4	0 ± 3
$4p\pi$	14	134722.0	0.3	1.00	1.0 ± 0.2			
$12p\pi$	8	**134766.6**	0.5	0.31	0.5 ± 0.1			100
$13p\pi$	8	**134875.0**	-0.9	0.32	[e]			100
$8p\pi$	9	134938.1	0.6	0.89	0.7 ± 0.1			100
$9p\pi$	9	135284.0	0.1	0.83	0.8 ± 0.1			100
$5p\pi$	12	135341.6	0.7	1.12	1.6 ± 0.3	51 ± 6	0 ± 9	49 ± 9
$7p\pi$	10	135470.3	-0.9	0.98	1.2 ± 0.2	58 ± 4	0 ± 9	42 ± 9
$4p\pi$	15	135470.6	-2.5	0.30	[e]			
$6p\pi$	11	135685.7	2.5	1.11	1.0 ± 0.4			100
$4p\pi$	16	**136160.4**	1.6	1.39	1.2 ± 0.1	100*		
$5p\pi$	13	136215.3	0.0	0.63	0.9 ± 0.1	100*		
$6p\pi$	12	136611.1	2.0	0.68	0.6 ± 0.1			100
$4p\pi$	17	**136792.6**	0.3	0.64	0.7 ± 0.1	100*		
$5p\pi$	14	137024.2	-0.4	0.62	1.1 ± 0.2	100*		

Table 3. Same as Table 1 for the $Q(3)$ transitions

	v	$Q(3)$ (obs) [a]	$obs-calc$	A_{calc} [b]	A_{obs}	γ_{diss} [c]	γ_{fluo}	γ_{ion}
$10p\pi$	0	**123485.1**[d,f]	0.8	0.33	0.2 ± 0.2			
$11p\pi$	0	**123671.9**	1.7	0.28	4.2 ± 0.7	12 ± 3	88 ± 9	
$12p\pi$	0	**123811.6**	-0.5	0.24	[e]			
$4p\pi$	4	123919.3	0.3	23.93	[e]	12 ±1	88 ± 3	
$7p\pi$	1	123949.04	0.5	2.25	[e]			
$8p\pi$	1	**124455.0**	-0.4	1.98	2.4 ± 0.3	14 ± 3	44 ± 7	42 ± 5
$6p\pi$	2	124678.6	0.2	7.88	10.1 ± 1.3	1 ± 1	17 ± 5	82 ± 6
$9p\pi$	1	**124804.2**	-0.8	1.18	1.2 ± 0.4	0 ± 3	5 ± 14	94 ± 17
$5p\pi$	3	124851.6	-0.4	10.54	12.4 ± 1.8	14 ± 1	71 ± 5	15 ± 5
$10p\pi$	1	**125055.8**	0.4	0.89	[e]			100
$11p\pi$	1	**125241.2**	-0.1	0.80	[e]		1 ± 0	
$4p\pi$	5	125248.9	-0.2	18.87	20.7 ± 3.6	13 ± 3	86 ± 7	2 ± 1
$12p\pi$	1	**125382.5**	-0.4	0.65	0.5 ± 0.2	100		
$7p\pi$	2	**125456.8**	0.6	3.90	[e]			
$8p\pi$	2	**125962.9**	0.2	2.74	3.1 ± 1.1	18 ± 6	12 ± 12	73 ± 18
$6p\pi$	3	126123.8	0.5	8.34	[e]			
$5p\pi$	4	126239.0	-0.3	9.41	7.5 ± 4.0		41 ± 7	59 ± 7
$4p\pi$	6	126519.6	0.3	15.24	16.5 ± 2.3	9 ± 1	86 ± 5	5 ± 1
$10p\pi$	2	**126562.4**	0.3	1.33	1.6 ± 0.3			1 ± 0
$12p\pi$	2	**126888.4**	-0.2	1.99	2.2 ± 0.5			100
$7p\pi$	3	**126901.5**	-0.6	3.29	[e]			100
$8p\pi$	3	**127406.6**	0.3	4.18	3.0 ± 1.0			100
$6p\pi$	4	127505.05	0.2	11.37	7.7 ± 33.0	8 ± 1	34 ± 8	58 ± 10
$5p\pi$	5	127567.4	-0.6	5.87	5.5 ± 1.8	16 ± 4	83 ± 11	0±15
$4p\pi$	7	127730.6	-0.3	11.12				

[a] observed transition energy, in cm^{-1}.
[b] A, emission probability for the transition to $X^1\Sigma_g^+, v''=0, N''=N$, in 10^6 s^{-1}.
[c] γ, experimental decay branching ratio in %.
[d] The positions of the upper state energy levels above the $v''=0, N''=0$ ground state level are obtained by adding the ground-state rotational energy 357.25 cm^{-1} ($N''=3$) [25] to the transition energy.
[e] Blended line.
[f] Transition energies in boldface correspond to new assignments.
* Dissociation into D($n=3$)+D($n=1$).
# This line is calculated as a single transition, but is observed split into two components, cf. the text.

Table 3 (continued)

	v	$Q(3)$ (obs) [a]	$obs-calc$	A_{calc} [b]	A_{obs}	γ_{diss} [c]	γ_{fluo}	γ_{ion}
$10p\pi$	3	**128005.3**	-0.5	1.57	1.9 ± 0.8			100
$11p\pi$	3	**128191.1**	-0.1	1.37	1.8 ± 0.8			100
$7p\pi$	4	**128284.2**	-0.1	4.51	[e]			100
$19p\pi$	3	**128782.0**	0.3	2.32	1.8 ± 1.6			100
$8p\pi$	4	**128787.2**	0.3	7.28	[e]			
$5p\pi$	6	128813.1	0.2	11.58	10.5 ± 1.8			
$4p\pi$	8	128886.6	0.2	6.10	6.2 ± 1.6		100 ±8	
$9p\pi$	4	**129138.3**	0.0	1.89	2.2 ± 0.5			100
$10p\pi$	4	**129388.3**	0.4	1.57	1.6 ± 0.5			100
$11p\pi$	4	**129572.9**	0.0	1.75	1.5 ± 0.4			100
$7p\pi$	5	**129607.4**	-0.4	3.43	4.9 ± 0.9			93 ± 12
$4p\pi$	9	129972.9	-0.1	11.64	[e]		33 ±4	67 ±4
$5p\pi$	7	**130036.4**	1.3	5.66	[e]			
$6p\pi$	6	**130099.7**	-0.3	3.24	4.0 ± 1.1			100
$9p\pi$	5	**130460.4**	-0.0	1.52	2.8 ± 2.5			100
$10p\pi$	5	**130709.8**	-0.1	1.44	1.3 ± 0.4			100
$7p\pi$	6	**130869.5**	-0.6	3.96	4.4 ± 0.7			100
$4p\pi$	10	131013.3	-0.0	6.43	8.5 ± 2.3	9 ± 1	62 ± 5	28 ± 7
$12p\pi$	5	**131036.8**	0.2	0.70	1.6 ± 0.7	67 ± 10		
$5p\pi$	8	**131185.6**	0.3	5.02	4.9 ± 1.0	5 ± 3	8 ± 9	87 ± 12
$9p\pi$	6	131723.4	-0.0	1.22	1.0 ± 0.6			100
$10p\pi$	6	**131972.2**	-0.4	1.37	[e]			
$4p\pi$	11	131992.4	-1.7	4.32#	3.0 ± 1.2	16 ± 6	85 ± 9	0 ±15
	11	**131995.9**	1.9	4.32#	2.4 ± 1.2	29 ± 17	65 ± 30	0 ± 7
$7p\pi$	7	**132076.4**	0.1	2.56	3.7 ± 0.7			100
$5p\pi$	9	**132279.5**	0.9	3.69	3.7 ± 0.9			92 ± 23
$6p\pi$	8	**132454.8**	-0.4	2.41	2.3 ± 0.8			100
$8p\pi$	7	**132582.2**	0.2	1.09	1.5 ± 0.5			100
$4p\pi$	12	132916.3	-0.7	3.12	3.3 ± 1.4	20 ± 7	67 ± 12	18 ± 19
$7p\pi$	8	**133224.4**	-0.1	2.02	2.0 ± 0.5			100
$5p\pi$	10	**133316.0**	0.7	2.44	2.3 ± 0.7	8 ± 1		92 ± 1
$12p\pi$	7	**133503.8**	0.1	0.58	0.7 ± 0.2			100
$6p\pi$	9	**133546.0**	-0.6	1.84	2.3 ± 0.4			100
$8p\pi$	8	**133729.8**	0.4	1.03	1.2 ± 1.6			100
$4p\pi$	13	**133778.0**	-4.2	2.01	2.1 ± 0.9		100	
$9p\pi$	8	**134076.0**	0.5	0.95	1.2 ± 0.3			100
$5p\pi$	11	**134290.5**	0.7	3.44	3.7 ± 0.7	5 ± 2		93 ± 2
$6p\pi$	10	**134578.5**	-2.0	2.24	1.7 ± 0.2	100 ±7*		

Table 4. Same as Table 1 for the $Q(4)$ transitions

	v	$Q(4)$ (obs) [a]	$obs-calc$	A_{calc} [b]	A_{obs}	γ_{diss} [c]	γ_{fluo}	γ_{ion}
$4p\pi$	4	123782.9[d]	0.1	23.85	26.0± 3.1	11 ± 2	89 ± 4	
$7p\pi$	1	**123824.4**[f]	0.1	2.30	2.2± 2.2	58 ± 12	42 ± 11	
$8p\pi$	1	**124331.0**	-0.3	1.65	2.1± 0.7	0 ±0	100 ± 12	
$6p\pi$	2	124549.0	-1.0	7.90	6.6± 0.9		100 ± 7	
$5p\pi$	3	124719.2	-0.3	10.48	13.0± 2.1	13 ± 2	72 ± 7	15 ± 5
$4p\pi$	5	125109.5	0.6	19.10	21.6± 4.2	9 ± 7	91 ± 8	
$11p\pi$	1	**125117.3**	0.3	0.66	0.6± 0.2			100
$7p\pi$	2	**125327.5**	-0.3	3.88	4.7± 1.8			90 ± 10
$8p\pi$	2	**125834.1**	0.4	3.06	2.7± 0.7			100
$6p\pi$	3	125990.5	-0.2	9.13	16± 3		16 ± 13	84 ± 5
$5p\pi$	4	**126102.4**	-0.5	9.33	10± 3	9 ± 5	42 ± 6	48 ± 12
$9p\pi$	2	**126183.0**	-0.4	1.54	3.5± 1.0	20 ± 6	5 ± 7	74 ± 12
$4p\pi$	6	126375.1	-0.1	15.22	16± 3	11 ± 2	89 ± 6	0 ± 2
$10p\pi$	2	**126433.4**	-0.1	1.33	1.4± 0.4			100
$11p\pi$	2	**126618.7**	-0.5	1.12	1.6± 0.5			100
$12p\pi$	2	**126759.9**	0.4	2.50	2.8± 0.7			100
$7p\pi$	3	**126770.2**	0.4	2.76	3.2± 1.2		47 ± 18	53 ± 14
$8p\pi$	3	**127274.1**	0.4	4.08	7± 2			100
$6p\pi$	4	127368.1	0.3	11.71	9± 2	6 ± 4	31 ± 12	63 ± 10
$5p\pi$	5	127427.4	-0.4	5.63	4.0± 1.3	0 ± 11	100 ± 19	0 ± 11
$4p\pi$	7	127582.9	0.0	11.02	12.6± 2.3	9 ± 2	87 ± 4	3 ± 3
$7p\pi$	4	**128147.4**	-0.2	4.47	4.7± 3.6			100
$12p\pi$	3	**128200.7**	0.3	0.65	0.8± 0.2			100
$8p\pi$	4	**128647.6**	0.2	8.84	8.8± 1.2			100
$19p\pi$	3	**128651.1**	0.2	2.69	2.1± 0.6			100
$5p\pi$	6	**128670.8**	0.4	10.04	[d]			

[a] observed transition energy, in cm^{-1}.

[b] A, emission probability for the transition to $X^1\Sigma_g^+, v''=0, N''=N$, in 10^6 s^{-1}.

[c] γ, experimental decay branching ratio in %.

[d] The positions of the upper state energy levels above the $v''=0, N''=0$ ground state level are obtained by adding the ground-state rotational energy 593.64 cm^{-1} ($N''=4$) [25] to the transition energy.

[e] Blended line.

[f] Transition energies in boldface correspond to new assignments.

* Dissociation into D($n=3$)+D($n=1$).

Table 4 (continued)

	v	$Q(4)$ (obs) [a]	$obs-calc$	A_{calc} [b]	A_{obs}	γ_{diss} [c]	γ_{fluo}	γ_{ion}
$4p\pi$	8	128735.4	0.4	6.31	7 ± 1	15 ± 3	85 ± 4	
$9p\pi$	4	**129001.6**	0.1	1.90	2.4 ± 0.5			100
$10p\pi$	4	**129251.9**	0.8	1.57	1.4 ± 0.4			100
$11p\pi$	4	**129436.4**	0.4	1.83	1.9 ± 0.5			100
$7p\pi$	5	**129467.7**	0.4	3.34	2.8 ± 2.5			100
$4p\pi$	9	129817.9	0.1	11.04	[e]		43 ± 5	57 ± 8
$5p\pi$	7	**129886.6**	-0.2	5.75	[e]			
$17p\pi$	4	**129952.0**	-0.1	1.57	1.6 ± 0.7			100
$6p\pi$	6	**129955.8**	-0.5	2.34	[e]			
$9p\pi$	5	**130320.2**	0.6	1.56	2.1 ± 0.4			100
$10p\pi$	5	**130569.2**	0.1	1.44	1.6 ± 0.9			100
$7p\pi$	6	**130725.1**	-0.5	3.90	4.3 ± 0.7			100
$4p\pi$	10	130854.2	0.5	6.37	5.4 ± 1.8	11 ± 3	66 ± 5	22 ± 5
$5p\pi$	8	**131030.8**	-2.4	4.97	3.5 ± 1.9			100 ±14
$6p\pi$	7	**131157.8**	-0.4	3.34	2.9 ± 0.7			100
$10p\pi$	6	**131827.8**	0.0	2.14	3.7 ± 1.2			
$4p\pi$	11	**131830.6**	-0.1	3.52	4.1 ± 3.2	2 ± 1	10 ± 5	89 ± 4
$7p\pi$	7	**131927.5**	-0.4	2.58	2.8 ± 1.4			100
$11p\pi$	6	**132013.6**	-0.1	0.70	0.6 ± 0.5			100
$5p\pi$	9	**132116.9**	-5.8	3.71				
$6p\pi$	8	**132302.5**	-0.5	2.38	2.0 ± 0.5			100
$15p\pi$	6	**132422.1**	-0.3	0.60	0.9 ± 0.3			100
$8p\pi$	7	**132433.5**	-0.2	1.01	1.3 ± 0.6			100
$4p\pi$	12	132748.8	-0.9	3.03	4.9 ± 1.3		70 ± 8	30 ± 4
$9p\pi$	7	**132780.1**	0.4	1.06	1.3 ± 0.7			100
$7p\pi$	8	**133072.0**	-0.2	2.03	1.3 ± 0.7			100
$6p\pi$	9	**133389.9**	-0.7	1.81	1.1 ± 7.3			
$4p\pi$	13	**133604.9**	-6.2	1.93	1.9 ± 0.7		100±13 *	
$5p\pi$	11	**134128.7**	1.6	3.20	2.1 ± 0.7			100 ± 7

Table 5. Same as Table 1 for the $Q(5)$ transitions

	v	$Q(5)$ (obs) [a]	$obs-calc$	A_{calc} [b]	A_{obs}	γ_{diss} [c]	γ_{fluo}	γ_{ion}
$4p\pi$	4	123614.2 [d]	0.2	24.01	43 ± 10		100	
$7p\pi$	1	**123670.8**[f]	0.5	2.26	3.6 ± 1.3	100		
$6p\pi$	2	**124390.4**	−0.4	7.94	10 ± 2			
$5p\pi$	3	**124554.5**	−1.1	10.40	12 ± 4	16 ± 3	28 ± 26	
$4p\pi$	5	124935.0	0.1	19.01	21 ± 5		100	
$7p\pi$	2	**125168.0**	−0.5	3.84	4.6 ± 1.7			100
$6p\pi$	3	**125825.9**	−0.2	9.14	16 ± 4			100
$5p\pi$	4	**125933.4**	−0.5	9.26	16 ± 8	[e]		
$4p\pi$	6	126196.7	0.4	15.24	23 ± 7		85 ± 9	
$8p\pi$	3	**127109.5**	0.0	3.56	3.8 ± 2.2			100
$6p\pi$	4	**127197.9**	−0.2	12.07	6 ± 3			67 ± 22
$4p\pi$	7	127398.3	−0.9	10.89	9 ± 4		100 ± 34	
$7p\pi$	4	**127977.9**	−0.4	4.43	6 ± 3			100
$8p\pi$	4	**128476.4**	−0.6	15.24	18 ± 7			72 ± 27
$4p\pi$	8	128547.8	−0.5	2.88	4.4 ± 1.7		100	
$9p\pi$	4	**128832.7**	0.6	1.90	2.5 ± 2.2		100	
$10p\pi$	4	**129082.0**	0.3	1.57	0.9 ± 0.6			100
$4p\pi$	9	129624.7	−0.2	10.54	14 ± 5		78 ± 9	22 ± 9
$5p\pi$	7	**129702.2**	−0.9	5.88	9 ± 3	60 ± 10		40 ± 10
$7p\pi$	6	**130546.5**	−0.2	3.85	3.7 ± 2.0			100
$4p\pi$	10	130655.1	−0.7	6.35	8.4 ± 3.5		100	
$5p\pi$	8	**130843.3**	−1.6	4.83	5.4 ± 3.2			100

[a] observed transition energy, in cm^{-1}.
[b] A, emission probability for the transition to $X^1\Sigma_g^+, v''=0, N''=N$, in 10^6 s^{-1}.
[c] γ, experimental decay branching ratio in %.
[d] The positions of the upper state energy levels above the $v''=0, N''=0$ ground state level are obtained by adding the ground-state rotational energy 887.08 cm^{-1} ($N''=5$) [25] to the transition energy.
[e] Blended line.
[f] Transition energies in boldface correspond to new assignments.